

HIGH LEVEL *ab initio* QUANTUM CHEMISTRY  
IN MAIN GROUP STUDIES

by

STEFAN ALEXANDER VOGT GEISSE

(Under the direction of Henry F. Schaefer III)

ABSTRACT

Quantum mechanical *ab initio* methods are employed to study molecules contain germanium and phosphorus. The dependence of the relative energies of 116 diphosphene and diphosphenylidene compounds on the modification of their structures is studied theoretically. Optimized geometries and relative energies are reported for all structures. In the case of the substitution of both H atoms by lithoxy (OLi) or ONa groups is the diphosphenylidene type structure found to be lower in energy. This result is explained through the natural population analyses, where a very favorable coulombic attraction is found in the OLi substituted diphosphenylidene structure. Next, a theoretical investigation of  $\text{Ge}_2\text{CH}_2$  is carried out. The singlet potential energy surface (PES) is systematically explored and energies were obtained using theoretical methods including coupled cluster theory and focal point analysis (FPA). Eleven stationary points are located on the  $\text{Ge}_2\text{CH}_2$  singlet ground state PES. Among them, seven structures are minima (**1S–7S**). The global minimum is predicted to be the hydrogen-bridged structure **1S**.

INDEX WORDS:     main group chemistry, isodesmic reaction, natural bond orbital,  
                          stochastic search, coupled cluster theory, focal point analysis,  
                          three-center two-electron bond, aromaticity

HIGH LEVEL *ab initio* QUANTUM CHEMISTRY  
IN MAIN GROUP STUDIES

by

STEFAN ALEXANDER VOGT GEISSE

B.A., Pontificia Universidad Católica de Chile, 2008

A Dissertation Submitted to the Graduate Faculty  
of The University of Georgia in Partial Fulfillment  
of the

Requirements for the Degree

DOCTOR OF PHILOSOPHY

ATHENS, GEORGIA

2013

©2013

Stefan Alexander Vogt Geisse

All Rights Reserved

HIGH LEVEL *ab initio* QUANTUM CHEMISTRY  
IN MAIN GROUP STUDIES

by

STEFAN ALEXANDER VOGT GEISSE

Approved:

Major Professor: Henry F. Schaefer III

Committee: Paul von Rague Schleyer  
Geoffrey Smith

Electronic Version Approved:

Maureen Grasso  
Dean of the Graduate School  
The University of Georgia  
May 2013



# High level *ab initio* Quantum Chemistry in Main Group Studies

Stefan Alexander Vogt Geisse

May 3, 2013

The mind, once stretched by a new idea, never returns to its original dimensions.

–Ralph Waldo Emerson

“ You can know the name of a bird in all the languages of the world, but when you’re finished, you’ll know absolutely nothing whatever about the bird. . . So let’s look at the bird and see what it’s doing – that’s what counts. I learned very early the difference between knowing the name of something and knowing something.”

–Richard Feynman

# Acknowledgments

Primarily, I would like to thank my parents Patricia and Nikolaus for their constant support and motivation, that allowed me to get to this point. Also my siblings, Katia, Thomas, and Clemens on which I know I can always rely.

On a more scientific note, I am very grateful to Prof. Alejandro Toro-Labbe, who was my first scientific mentor and the person that facilitated my arrival at CCQC. Of course, I am indebted to Dr. Schaefer who took me in his scientific heaven called CCQC and allowed me to pursue my research interests. I am also thankful to Dr. Yukio Yamaguchi and Dr. Andy Simmonett for being always extremely helpful and sharing their vast knowledge with me. I also have to mention my committee members Dr. Schleyer and Dr. Smith and acknowledge that they did a good job at preparing me for the real scientific world. I have to thank the current and previous CCQC members for creating a great and friendly environment.

I had the opportunity to meet great people and make many new friends. In that sense I especially have to mention Alex Sokolov for being an outstanding collaborator and friend, Shane McNew for his unconditional friendship, and Jay Agarwal for long nights in the office and many fun nights out. Finally, over the last four years I made many friends from many different countries in this beautiful city of Athens, who made my stay here ever so enjoyable.

# Contents

<b>Acknowledgments</b>	<b>iv</b>
<b>1 Introduction and Background</b>	<b>1</b>
1.1 Theoretical Methods . . . . .	1
1.2 Main Group Chemistry . . . . .	12
1.3 Research Overview . . . . .	13
<b>2 Reducing and Reversing the Diphosphene-Diphosphenylidene Energy Ordering</b>	<b>15</b>
2.1 Introduction . . . . .	16
2.2 Theoretical Methods . . . . .	17
2.3 Results and Discussion . . . . .	19
2.4 Conclusions . . . . .	35
2.5 Acknowledgments . . . . .	35
<b>3 Structure, Bonding and Aromaticity of <math>\text{Ge}_2\text{CH}_2</math></b>	<b>36</b>
3.1 Introduction . . . . .	36
3.2 Theoretical Procedures . . . . .	38
3.3 Results and Discussion . . . . .	42
3.4 Natural Bond Orbital Analyses . . . . .	57

3.5	Aromaticity . . . . .	62
3.6	Concluding Remarks . . . . .	64
3.7	Acknowledgments . . . . .	64
<b>4</b>	<b>Summary and Conclusions</b>	<b>65</b>
	<b>Bibliography</b>	<b>67</b>
	<b>Appendices</b>	<b>78</b>
<b>A</b>	<b>Supporting Information for Chapter 3</b>	<b>79</b>
A.1	Focal point table for stationary points <b>4S- SSP2</b> . . . . .	79
A.2	Natural Bond Orbital Analysis . . . . .	83

# List of Figures

2.1	Isodesmic reactions for evaluating energetic effects related to the substitution of one or two hydrogens of diphosphene and diphosphinylidene. Through these equations it is possible to separate the substituent effects on the two isomers, making it easier to study the energetics of single and double substitution. . .	18
2.2	Theoretical geometries for representative diphosphinylidenes $R_2PP$ with $R = H, OLi, OH, OF, CN, F$ . Bond distances are reported in Å. As seen in Table 2 and 3, sixteen other structures with different substituents $R$ were also studied	21
2.3	Theoretical geometries for representative diphosphenes $RPPR$ with $R = H, OLi, OH, OF, CN, F$ . Bond distances are reported in Å. As seen in Table 2 and 3, sixteen other structures with different substituents $R$ were also studied	22
2.4	Plot of the doubly (doub) substituted diphosphinylidene-diphosphene energy gap $\Delta E_{doub} = E(R_2P=P) - E(RP=PR)$ against the reaction energies for isodesmic reaction $R - PH_2 + HRP = P \rightarrow R_2P = P + PH_3$ . The good correlation between $\Delta E(R4)$ and $\Delta E_{doub}$ indicates that the reduction of the energy difference between diphosphene and diphosphinylidene isomers is mainly due to a favorable substituent effect after the incorporation of the second substituent into the parent diphosphinylidene compound. . . . .	29

3.1	Geometry of the Ge <sub>2</sub> CH <sub>2</sub> global minimum structure <b>1S</b> ( <i>C</i> <sub>2v</sub> symmetry) optimized at the CCSD(T)/cc-pVQZ level of theory (on the left). Plots of its CASSCF frontier natural orbitals are shown on the right. The symmetries and the occupancies of three natural orbitals are also shown. . . . .	47
3.2	Geometry of the Ge <sub>2</sub> CH <sub>2</sub> isomer <b>2S</b> ( <i>C</i> <sub>s</sub> symmetry) optimized at the CCSD(T)/cc-pVQZ level of theory (on the left). Plots of its CASSCF frontier natural orbitals are shown on the right. The energy relative to the global minimum <b>1S</b> is computed at the CCSDT(Q)/CBS level of theory. The symmetries and the occupancies of four natural orbitals are also shown. . . . .	47
3.3	Geometry of the Ge <sub>2</sub> CH <sub>2</sub> isomer <b>3S</b> ( <i>C</i> <sub>s</sub> symmetry) optimized at the CCSD(T)/cc-pVQZ level of theory (on the left). Plots of the CASSCF frontier natural orbitals are shown on the right. The energy relative to the global minimum <b>1S</b> is computed at the CCSDT(Q)/CBS level of theory. The symmetries and the occupancies of four natural orbitals are also shown. . . . .	48
3.4	Geometries of the isomers <b>4S-7S</b> optimized at the CCSD(T)/cc-pVQZ level of theory. . . . .	48
3.5	Geometries of the transition states <b>TS1-TS2</b> , and second-order saddle points <b>SSP1-SSP2</b> optimized at the CCSD(T)/cc-pVQZ level of theory. . . . .	49
3.6	Depiction of the bonding structures predicted by the NBO analyses. Upper panel: Lewis type structures for the three lowest lying isomer <b>1S,2S</b> , and <b>3S</b> . Middle panel: The Ge-H-Ge three-center two-electron bond on <b>1S</b> , the Ge1-Ge2 $\sigma$ -bond, the Ge1-H bond on <b>2S</b> and the radial in plane three-center two-electron Ge-C-Ge bond on <b>3S</b> . Lower panel: The out-of-plane three-center two-electron $\pi$ -bonds for <b>1S, 2S</b> , and <b>3S</b> . . . . .	61

3.7	NICS(0) and NICS(0) <sub><math>\pi_{zz}</math></sub> values in ppm for the isomers <b>1S</b> , <b>2S</b> and <b>3S</b> taken at the center of the rings. A negative NICS(0) value indicates diatropic shielding and aromaticity. The orbitals used to compute the dissected NICS(0) <sub><math>\pi_{zz}</math></sub> are also shown. . . . .	63
-----	--	----



# List of Tables

2.1	Energy differences (kcal/mol) between the monosubstituted RHPP and RPPH isomers ( $\Delta E_{sing}$ ) and between disubstituted R <sub>2</sub> PP and RPPR ( $\Delta E_{doub}$ ). . . .	23
2.2	Isodesmic reaction energies (kcal/mol) for the singly substituted diphosphenes and diphosphinylienes: . . . . .	27
2.3	Isodesmic reaction energies (kcal/mol) for the doubly substituted diphosphenes and diphosphinylienes: . . . . .	28
2.4	Wiberg bond orders for R <sub>2</sub> PP and RPPR structures. . . . .	33
2.5	Natural atomic charges from NPA for the doubly substituted isomers. In parentheses are the charges for the singly substituted isomer. . . . .	34
3.1	Focal Point Analysis of the Relative Energy Between Isomers <b>1S</b> and <b>2S</b> ( $\Delta E_{final}$ , kcal mol <sup>-1</sup> ). <sup>a</sup> . . . . .	49
3.2	Focal Point Analysis of the <b>3S</b> Isomer Relative Energy of Ge <sub>2</sub> CH <sub>2</sub> ( $\Delta E_{final}$ , kcal mol <sup>-1</sup> ). <sup>a</sup> . . . . .	50
3.3	The FPA extrapolated and final corrected energies (in kcal mol <sup>-1</sup> ) for the eleven stationary points located on the singlet Ge <sub>2</sub> CH <sub>2</sub> potential energy surface	50
3.4	Harmonic vibrational frequencies (in cm <sup>-1</sup> ) and the ZPVE (in kcal mol <sup>-1</sup> ) for the 11 Ge <sub>2</sub> CH <sub>2</sub> structures at the CCSD(T) cc-pVQZ level of theory . . . . .	56
A.1	Focal point table for the <b>4S</b> isomer . . . . .	79

A.2	Focal point table for the <b>5S</b> isomer . . . . .	80
A.3	Focal point table for the <b>6S</b> isomer . . . . .	80
A.4	Focal point table for the <b>7S</b> isomer . . . . .	80
A.5	Focal point table for the <b>TS1</b> stationary point . . . . .	81
A.6	Focal point table for the <b>TS2</b> stationary point . . . . .	81
A.7	Focal point table for the <b>SSP1</b> stationary point . . . . .	81
A.8	Focal point table for the <b>SSP2</b> stationary point . . . . .	82
A.9	Natural bond orbitals for isomer <b>1S</b> obtained at the B3LYP/def2-TZVP level of theory . . . . .	83
A.10	Natural bond orbitals for isomer <b>2S</b> obtained at the B3LYP/def2-TZVP level of theory . . . . .	83
A.11	Natural bond orbitals for isomer <b>3S</b> obtained at the B3LYP/def2-TZVP level of theory . . . . .	84

# Chapter 1

## Introduction and Background

### 1.1 Theoretical Methods

#### 1.1.1 Foundations of Quantum Chemistry

Small objects such as atoms and molecules follow the laws of quantum mechanics. In order to obtain the energy and other properties of a N-electron molecular system, the time-independent non-relativistic Schroedinger equation<sup>1</sup> must be solved:

$$\mathcal{H}\Psi = \mathcal{E}\Psi, \quad (1.1)$$

where  $\Psi$  is the N-electron wavefunction and  $\mathcal{H}$  the Hamiltonian operator given by:

$$\mathcal{H} = \sum_{i=1}^N \frac{1}{2} \nabla_i^2 - \sum_{i=1}^N \frac{1}{2M_A} \nabla_i^2 - \sum_{i=1}^N \sum_{A=1}^M \frac{Z_A}{r_{iA}} + \sum_{i=1}^N \sum_{j>i}^N \frac{1}{r_{ij}} + \sum_{A=1}^M \sum_{B>A}^M \frac{Z_A Z_B}{R_{AB}}. \quad (1.2)$$

The physical entities contained in the Hamiltonian are kinetic energy and potential energy interactions. Since nuclei are much heavier and move more slowly than electrons one

can consider the electrons as moving in the field of fixed nuclei. This is called the Born-Oppenheimer approximation<sup>2</sup> and, effectively decouples nuclear and electronic motion such that the Schrödinger equation becomes:

$$\mathcal{H}_{elec}\Psi(\mathbf{r};\mathbf{R}) = \mathcal{E}_{elec}\Psi(\mathbf{r};\mathbf{R}), \quad (1.3)$$

$$\mathcal{H}_{elec} = \sum_{i=1}^N \frac{1}{2} \nabla_i^2 - \sum_{i=1}^N \frac{1}{2M_A} \nabla_i^2 - \sum_{i=1}^N \sum_{A=1}^M \frac{Z_A}{r_{iA}} + \sum_{i=1}^N \sum_{j>i}^N \frac{1}{r_{ij}}, \quad (1.4)$$

and only depends parametrically on the nuclear positions. The total energy is obtained after adding the nuclear repulsion constant:

$$E_{tot} = \mathcal{E}_{elec} + \sum_{A=1}^M \sum_{B>A}^M \frac{Z_A Z_B}{R_{AB}}. \quad (1.5)$$

The solution to this equation provides the energy and wavefunction of a molecular system for a given nuclear orientation. The electronic wavefunction which represents a stationary state of a molecule is given by:

$$\Psi(\mathbf{r}_1, \mathbf{r}_2, \dots, \mathbf{r}_N), \quad (1.6)$$

where  $\mathbf{r}_i$  are the coordinates (spatial and spin) of the N electrons. The most straightforward way of constructing such a wavefunction is as product of one electron wavefunctions (spin-orbitals):

$$\Psi(\mathbf{r}_1, \mathbf{r}_2, \dots, \mathbf{r}_N) = \psi(\mathbf{r}_1)\psi(\mathbf{r}_2)\cdots\psi(\mathbf{r}_N), \quad (1.7)$$

However this wavefunction is physically flawed, since it does not consider electrons as indistinguishable and interacting entities. Also given that electrons are fermions, this wave-

function does not comply with the antisymmetry postulate. A way to simultaneously satisfy the indistinguishability and antisymmetry requirements, is representing the N-electron wavefunction as a determinant:

$$\Psi(\mathbf{r}_1, \mathbf{r}_2, \dots, \mathbf{r}_N) = \frac{1}{\sqrt{N!}} \begin{vmatrix} \psi_1(\mathbf{r}_1) & \psi_2(\mathbf{r}_1) & \cdots & \psi_N(\mathbf{r}_1) \\ \psi_1(\mathbf{r}_2) & \psi_2(\mathbf{r}_2) & \cdots & \psi_N(\mathbf{r}_2) \\ \vdots & \vdots & & \vdots \\ \psi_1(\mathbf{r}_N) & \psi_2(\mathbf{r}_N) & \cdots & \psi_N(\mathbf{r}_N) \end{vmatrix}. \quad (1.8)$$

The Slater determinant<sup>3</sup> is a much improved wavefunction, since electrons are indistinguishable. Moreover any interchange of particles leads to a sign change in the wavefunction, thus satisfying the antisymmetry postulate. A consequence that follows directly from the antisymmetry postulate is the Pauli exclusion principle<sup>4</sup>. If two electrons are in the same spin-orbital, two columns of the determinant are identical. Due to fundamental properties of a determinant this means that the wavefunction is equal to zero, thus effectively prohibiting that two electrons of the same spin occupy the same spin-orbital. Therefore a single Slater determinant is the simplest antisymmetric wavefunction, which can be used to describe the ground state of a N-electron system.

### 1.1.2 Hartree-Fock and Configuration Interaction Methods

The expectation value of the ground state energy is given by the integral:

$$E_0 = \langle \Psi_0 | \mathcal{H} | \Psi_0 \rangle. \quad (1.9)$$

The variational principle states that the best wavefunction is the one that results in the lowest possible energy. Thus, in the Hartree-Fock method, the energy is minimized with respect to the orbitals in the Slater determinant. The resulting equation is the Hartree-Fock

equation<sup>5-7</sup>, which determines the orbitals that yields the lowest energy.

$$f(i)\chi(\mathbf{x}_i) = \epsilon\chi(\mathbf{x}_i), \quad (1.10)$$

where  $f(i)$  is an effective one electron operator called Fock operator:

$$f(i) = -\frac{1}{2}\nabla_i^2 - \sum_{A=1}^M \frac{Z_A}{r_{iA}} + v^{HF}(i), \quad (1.11)$$

where  $v^{HF}(i)$  is the average potential experienced by the  $i$ -th electron. Since the expression of the potential depends on the orbitals, this integro-differential equation is self-consistent and has to be solved iteratively. In practice, the orbitals used are a finite expansion of a set of basis functions and a matrix eigenvalue equation for the expansion coefficients is obtained. This results in a set of matrix equations called the Roothaan equations<sup>8,9</sup> that can be solved using standard matrix techniques. The allure of the Hartree-Fock methods lies in the reduction of a complicated many-electron problem into a one-electron problem, thus providing a solid foundation for modern wavefunction methods. However, the Hartree-Fock method by itself fails in providing quantitative results in the range of chemical accuracy, since this method incurs in error by only accounting electron-electron interactions in an average way.

A higher degree of variational flexibility can be obtained by adding excited determinants to the wavefunction expansion. It can easily be shown that the exact wavefunction for the  $N$ -electron problem can be written as a linear combination of all possible  $N$ -electron Slater determinants<sup>10</sup>:

$$|\Phi\rangle = c_0 |\Psi_0\rangle + \sum_{ia} C_i^a |\Psi_i^a\rangle + \sum_{\substack{a<b \\ i<j}} C_{ij}^{ab} |\Psi_{ij}^{ab}\rangle + \sum_{\substack{a<b<c \\ i<j<k}} C_{ijk}^{abc} |\Psi_{ijk}^{abc}\rangle. \quad (1.12)$$

The lowest eigenvalue of the Hamiltonian matrix  $\langle \Phi | \mathcal{H} | \Phi \rangle$  is the exact ground state energy. Each of the excited determinants can be regarded as a possible electronic configuration of the N-electron system, thus the procedure is called configuration interaction (CI). Full CI is only feasible for molecules with very few electrons due to the rapid scaling of the method with the system size and basis set. Therefore, the aim of modern electronic structure methods is to be able to get as close as possible to this exact solution, while keeping the computational cost at a minimum. In that sense, the holy grail, to which all electronic structure methods aspire is to fully include the correlation energy. This elusive quantity is defined as the difference between the exact energy and the Hartree-Fock-limit energy:

$$E_{corr} = E_0 - E_{HF}. \quad (1.13)$$

Clearly, the correlation energy is not a physical observable which can be obtained by experiment. It solely, manifest the deficiencies of the Hartree-Fock method which are the lack of coulombic electron-electron interaction (dynamic correlation) and unphysical dissociation products and energies (static correlation).

### 1.1.3 Coupled Cluster Method

Ever since it was first introduced by Čížek and Paladus<sup>11</sup> coupled cluster has developed into the most reliable yet computationally affordable method to include electron correlation<sup>12,13</sup>. The wavefunction in the coupled cluster method is obtained using the exponential ansatz:

$$\Psi_{CC} = e^{\hat{T}} \Psi, \quad (1.14)$$

where  $\hat{T}$  is the excitation operator containing all levels of excitation. This wavefunction may be inserted in the Schroedinger equation,

$$\mathcal{H}e^{\hat{T}}\Psi_0 = Ee^{\hat{T}}\Psi_0, \quad (1.15)$$

and the energy can be obtained by left-projecting this equation by the reference,

$$E = \langle \Psi_0 | \mathcal{H}e^{\hat{T}} | \Psi_0 \rangle. \quad (1.16)$$

The advantage of this ansatz is that it yields a size-consistent energy, unlike configuration interaction methods, where size consistency is not ensured. Most commonly, truncated CC methods are employed. In the CCSD method<sup>14,15</sup> the cluster operators truncated to include only single and double excitations:

$$\hat{T} = \hat{T}_1 + \hat{T}_2. \quad (1.17)$$

Furthermore, the methods including triples and quadruples excitations are denominated CCSDT and CCSDTQ respectively. Currently, CCSD(T)<sup>16-19</sup> where triple excitations are included in a perturbative manner, is considered the “gold standard” when used in conjunction with a large basis set. However, since the method scales with  $O(N^7)$  (N is the number of basis functions) it is only feasible for relatively small systems.

### 1.1.4 Focal Point Analysis

Electronic structure methods aspire to get as close as possible to the exact solution of the Schrödinger equation embodied by the full-CI/infinite basis set wavefunction (*vide infra*). While the molecular geometries obtained at lower levels of theory are normally sufficiently accurate, the lack of electron correlation and too small basis sets, result in inaccurate energies. By means of focal point analysis<sup>20-23</sup> it is possible to systematically improve the molecular energy and advance towards the exact non-relativistic energy. This is accomplished by



performing single point energy computations at progressively elevated levels of theory and basis sets. The dependence of the energy on electron correlation is monitored by registering the energy change with increasing particle excitation order. On the other hand, Dunning's cc-pVXZ basis sets,<sup>24,25</sup> where X is the cardinal number indicating the maximum angular momentum, are employed to systematically increase the basis set size thereby diminishing the basis set error. The cc-pVXZ family of basis sets is especially suitable, since the increase in cardinal number is accompanied by additional angular momentum function on each shell. The systematic size increase is paramount in order to rigorously extrapolate to complete basis set. The basis set error arises due to a slow convergence of the orbital expansion, which makes the addition of high angular momentum functions indispensable. The main physical reason for this slow convergence can be attributed to the electron-electrons cusp<sup>26</sup>, which is manifested by a rapid decay of the wavefunction at the coalescence point of two electrons. This two-body effect is poorly described by a one-particle basis set expansion. Consequently, the basis set dependence is more prevalent in correlated wavefunctions, where the basis set error decays at a vexatiously sluggish rate of  $l^{-3}$  ( $l$  corresponds to the maximum angular momentum of the basis). Nonetheless, the extrapolation of the energy to complete basis set can be obtained by:

$$E_{corr}(X) = D + EX^{-3} \quad (1.18)$$

where D and E are parameters to be fit and the correlation energy at a complete basis is obtained by taking the limit of the expression for infinite angular momentum. In order to be able to obtain the fitting parameters, computations up to at least cc-pVQZ basis set is required. Since in the Hartree-Fock method no explicit electron-electron correlation is included, the wavefunction expansion converges exponentially and the energy dependence with basis set can be expressed as:

$$E_{HF}(X) = A + Be^{-CX} \quad (1.19)$$

where A B and C are fitting parameters, that can be calculated from computation with at least three different basis sets. The energy at complete basis set can be obtained by taking the limit of this expression, as the basis approaches infinity.

The shrewdness of the focal point approach comes from the additivity concept. For each layer of added correlation treatment, only the difference from the previous level is considered. In the hierarchy  $HF \rightarrow MP2 \rightarrow CCSD \rightarrow CCSD(T) \rightarrow CCSDT \rightarrow CCSDT(Q)$ , Hartree-Fock provides the reference energy and each subsequent level corrects for the additional particle rank. For example, the CCSD incremental correction to the MP2 energy is:

$$\delta[CCSD] = \Delta E_{CCSD} - \Delta E_{MP2} \quad (1.20)$$

Here the change should be rather small since most two body interactions are already accounted for in the MP2 energy corrections. The electron cusp is essentially a two electron phenomenon, the basis set dependence becomes less when correcting for three-body and four-body terms. Therefore, it is physically reasonable to assume that for the CCSD(T) and CCSDT(Q) the basis set is converged at smaller basis set sizes like cc-pVTZ and cc-pVDZ. Hence, the correction for three, four and higher body correlation effects at small basis sizes can be added without extrapolation to the extrapolated energy value to obtain the final focal point energy.

Using the focal point analysis, accuracies of 1 kcal/mol can be achieved, which can be further improved when adding relativistic,<sup>27</sup> diagonal Born-Oppenheimer<sup>28</sup> and core correlation corrections, to obtain subchemical accuracy in the order of 0.1 kcal/mol.

### 1.1.5 Density Functional Theory

The use of the electron density instead of the N-electron wavefunction as primary variable is the core concept of density functional theory (DFT).<sup>29</sup> The main advantage of using the electron density instead of the N-electron wavefunction is that the electron density is a function of the three spatial coordinates, rather than 3N coordinates. In the 1920s, Tomas and Fermi<sup>30,31</sup> were the first to recognize the potential use of the electron density in electronic structure theory, when they proposed to describe the electron density in an atom using statistical considerations. However, it was not till the 1960s that Kohn, Hohenberg and Sham transformed DFT into an exact and complete theory. In a landmark paper<sup>32</sup>, Hohnenberg and Kohn postulated two theorems. The first one states that any physical observable may be written as a functional of the electron density, as long as it is the ground state and the electron density integrates to the total number of electrons. This theorem implies a 1:1 mapping between the wavefunction and the electron density. The second theorem asserts that the exact electron density of a non-degenerate ground state may be obtained by the density that minimizes the energy. The latter theorem leads to the Euler-Lagrange equation:

$$\mu = \frac{\delta E_v[\rho]}{\delta \rho(\mathbf{r})} = v(\mathbf{r}) + \frac{\delta F_{HK}[\rho]}{\delta \rho(\mathbf{r})}, \quad (1.21)$$

where  $F_{HK}[\rho]$  is the Hohenberg-Kohn universal functional and  $v(\mathbf{r})$  is the external potential. This equation is central to DFT, since it provides a formula to minimize the energy to obtain the density of the ground state.

Kohn and Sham<sup>33</sup> proposed an elegant method to solve the Euler-Lagrange equations introducing a one-particle orbital basis set. Nonetheless, since the exact form of the universal functional is unknown approximations have to be undertaken. These approximation factor into the equations in the form of the exchange-correlation functional. Various forms for this functional have been proposed<sup>34-40</sup>, of which some contain an immoderate amount of

empirical parameters<sup>41</sup>. Therefore it is possible for one functional to perform well for a certain type of system (e.g. organic molecules), while delivering poor results for a system of a different nature (e.g. metal compounds). The B3LYP functional<sup>34,35</sup> is considered to be among the most popular functionals. It incorporates three parameters based on experimental data and has been proven to deliver very accurate ground state energies and molecular geometries at a cost comparable to a Hartree-Fock computations. In that sense, the great advantage of DFT is the incorporation of electron correlation in an inexpensive manner. However, care has to be taken when choosing an exchange-correlation functional, given the artisan and unmethodical way some of the functionals are constructed.

### 1.1.6 Natural Bond Orbital

*Ab initio* molecular orbital theory (*vide infra*) has been tremendously successful in determining the ground state energy and molecular structures of small molecules. However, in order to obtain insights about the underlying bonding motifs, further analysis of the wavefunction is necessary. For this reason, the electron density needs to be partitioned in a chemically meaningful way. The natural bond orbital (NBO) method<sup>42–45</sup> employs as a starting point the optimal Lewis structure representation<sup>46</sup> of shared and unshared electrons<sup>a</sup> for a given molecule. This represents an excellent model chemistry for well localized systems where up to 99.9% of the electron density may be accounted for by the “classical” two-center bond, lone pair picture. For more delocalized systems, a perturbative correction to the Lewis picture, in form of an orbital donor-acceptor interaction is added to obtain a succinct and chemically intuitive description of the electron density. In order to obtain a natural bond orbital basis, a sequence of transformations and orthogonalizations from the input basis set to a localized orbital picture has to be performed:

---

<sup>a</sup>Lewis proposed his theory 10 years(!) prior to the discovery of quantum mechanics, he speculated that the reason for electron pairing was a different coulomb law at small distances.

$$\text{input basis} \rightarrow \text{NAOs} \rightarrow \text{NHOs} \rightarrow \text{NBOs} \quad (1.22)$$

Each orbital set in this sequence can be written as a linear combination of orbitals in the preceding basis. For example, a typical NBO of a diatomic molecule A–B could be represented as:

$$\sigma_{AB} = c_A h_A + c_B h_B, \quad (1.23)$$

where  $h_A$  and  $h_B$  are natural hybrid orbitals (NHO) localized on the centers A and B respectively. Moreover, each of the hybrids is composed of a linear combination of natural atomic orbitals (NAO). It is important to observe that each step in the sequence represents a unitary transformation into an orthonormal set that spans the whole space of the input basis. The NBOs obtained from this routine correspond to the best (highest occupancy) Lewis type structures and they can be categorized into core orbitals, lone pairs and bonding orbitals. Furthermore if the occupancy of some NBOs is too low, the search can be extended to three-center bonds. Other chemically relevant interactions like resonance or hyperconjugation effects are accounted for through a perturbative correction to the localized picture. The resulting donor-acceptor interaction is between a filled and a virtual orbitals, and is necessarily an energy lowering interaction. Another feature that arises from this unitary transformation procedure is the natural population analysis<sup>47</sup>. The natural population  $q_i^{(A)}$  of an orbital corresponds to the diagonal density element in the NAO basis. The total charge on a atom can be obtained by:

$$q^{(A)} = \sum_i q_i^{(A)} \quad Q^{(A)} = Z_A - q^{(A)} \quad (1.24)$$

All together NBO provides valuable tools that lent support to a complete chemical interpretation of the bonding of a molecular system.

## 1.2 Main Group Chemistry

Despite its ubiquitousness, first row chemistry does not epitomize well the general bonding patterns of the main group elements, but rather represents an exception. Kutzelnigg<sup>48</sup> pointed out that this “anomalous” behaviour of first row atoms can be attributed to the similar radial extents of 2s and 1p orbitals. Only in the first row the p-orbitals have no lower shell of same angular momentum, thus making them more compact than higher level p-orbitals. The consequence is a good orbital size match and a preference for s- and p-orbital mixing. The energetic reasons for orbital mixing are threefold. First, the mixing of s- and p-orbitals enables the formation of stronger bonds due to a significant size increase of the hybrid bonding lobe. Second, the mixing of s-orbital lone pairs with p-orbitals reduces the Pauli repulsion with adjacent bonds, since it can direct the lone pair density to the opposite direction of the bond. Third, reduction of Pauli repulsion of neighbouring atoms due to increase of the angle size.

These points become less preponderant in higher row atoms, since p-orbitals are more diffuse than the compact s-orbitals. Hence no significant change in lobe size resulting in better overlap is achieved, making hybridization an unfavourable process. Furthermore, the atom size in higher row elements is larger than in the first row, making Pauli repulsion much less prevalent. Consequently hybridization in molecules containing higher row atoms is not longer paramount, and overall an energetically unfavourable process.

Another fundamental difference between higher main group elements and their lighter congeners is the energy of the  $\pi$ -bond. Whereas carbon favours the formation of multiple  $\pi$ -bonds, these are not present in the low energy structures of the analogous molecules of the higher row elements. This fundamental difference is due to the large jump in the covalent radii between C (0.77 Å) and Si (1.17 Å) or Ge (1.22 Å)<sup>49</sup>. Consequently, the overlap between the lobes of the p-orbitals is significantly reduced with relation to unsaturated hydrocarbon

species and the energy of the  $\pi$ -bond is considerably diminished. A prime example is  $X_2H_2$  ( $X = C, Si, Ge$ ). While acetylene has a linear structure and favours multiple  $\pi$ -bonds, silacteylen<sup>50</sup> and germaacetylen<sup>51</sup> do not form  $\pi$ -bonds but rather form 3-center 2-electron  $\sigma$ -bonds with two bridging hydrogen.

Nonetheless, experimental isolation of multiply bonded molecules containing silicon, germanium and phosphorus has been achieved using bulky substituents that are able to kinetically stabilize the double bond, thus avoiding the formation of singly bonded polymers or oligomers.<sup>52-56</sup> A consequence of the weak  $\pi$ -bonds is an increase in biradical and non-bonded electron pair character as the atom gets larger. Lately, several efforts have been made to use this particular trait of doubly bonded main group species, in reactions with small molecules in order to mimic reactivity patterns of transition metals<sup>57-60</sup>.

## 1.3 Research Overview

The theories and methods discussed above form the conceptual framework for this research. In the first part of this dissertation we have studied 116 substituted diphosphene (RPPR) and diphosphinylidene ( $R_2PP$ ) compounds in order to find a substituent that is capable of reversing the energy ordering among these two types of structures. A total of 29 different substituents are probed. Density functional theory is used to obtain geometries and relative energies. Finally isodesmic reactions and natural bond orbital analysis is presented in order to elucidate the reason of the varying energy gaps.

In the second part, a systematic study of the potential energy surface of the  $Ge_2CH_2$  system is presented. The potential energy surface is explored using a stochastic search procedure for the search of stationary points, followed by state of the art *ab initio* optimizations and energy computations. The resulting structures are further examined by natural bond orbital analysis, and aromaticity is probed for with the nuclear independent chemical shift

method. A brief summary is provided in Chapter 4.



## Chapter 2

# Reducing and Reversing the Diphosphene-Diphosphinylidene Energy Ordering

<sup>a</sup>

---

<sup>a</sup>S. Vogt-Geisse H.F. Schaefer, J. Chem. Theo. Comp. **8** 1663–1670 (2012) Reprinted here with the permission of the American Chemical Society

## 2.1 Introduction

Phosphorus chemistry has developed rapidly in the last two decades due to a plethora of interesting properties attributed to this family of compounds.<sup>61</sup> In the midst of this renaissance, secondary diphosphenes and diphosphinylidenes have received considerable attention due to their, for phosphorus compounds, unusual double bonds. This unique feature, can be utilized in a variety of applications ranging from novel electron-rich organometallic ligands<sup>62-64</sup> to potential hydrogen storage systems<sup>65</sup>. The synthesis and isolation of diphosphenes and especially diphosphinylidenes has been challenging since they tend to oligomerization or polymerization due to thermodynamic preferences<sup>66</sup>. However, stable phosphorus compounds with P=P double bonds have been obtained using bulky substituents, which make the compounds kinetically if not thermodynamically stable<sup>67-72</sup>. Thus a significant number of diphosphene-like compounds have been synthesized and their structures and reactivities have been examined. For example, Robinson and coworkers recently synthesized novel diphosphene compounds where the P-P fragment was stabilized by N-heterocyclic carbene donors.<sup>73</sup>

One of the characteristic features of the diphosphene compounds is the length of the P-P bond. It has been found that in bulky substituted diphosphenes, the length of the P-P bond lies in the range 2.001 to 2.034 Å, with phosphorus-phosphorus vibrational frequencies of about 610 cm<sup>-1</sup>, confirming the presence of a P=P double bond<sup>74</sup>. Furthermore, the recent important study by Partyka et al. showed that it is possible to further strengthen the double bond by reducing the distance between adjacent phosphorus atoms via auration of the P-P moiety of Mes\*P=P(AuCl)Mes\* (Mes\* = 2,4,6-tri-tert-butylphenyl) to a bond length of 1.975 Å<sup>75</sup>.

Despite the above, no success has been reported to date in the synthesis and isolation of a diphosphinylidene. It has been shown, however, that diphosphinylidene derivatives can coordinate to transition metals, primarily in an  $\eta^2$  or side-on fashion. The latter synthesis was

accomplished using phosphinophosphinidenephosphoranes [ $t\text{Bu}_2\text{P}-\text{P}=\text{P}(\text{X})t\text{Bu}_2$  X=Me,Br] and  $R_2\text{P}-\text{P}(\text{SiMe}_3)\text{Li}$  as precursors<sup>62,64</sup>.

Several theoretical studies have investigated the nature of diphosphene and diphosphinyldene type compounds<sup>65,76–80</sup>. The electronic ground state of  $\text{H}_2\text{PP}$  was long predicted to be a triplet<sup>77,78,81,82</sup>, but recent computations using the CCSD(T)/aug-cc-pVQZ level of theory find that the ground state appears to be of singlet nature with a triplet-singlet gap of 2.8 kcal/mol<sup>65</sup>. In addition, high level *ab initio* computations have shown that the energy gap between the ground state of *trans* diphosphene (HPPH) and *geminal* diphosphinyldene ( $\text{H}_2\text{PP}$ ) is about 25 kcal/mol<sup>83</sup>. Finally it has been demonstrated that  $\pi$ -donating and bulky substituents favor the planar singlet state of substituted diphosphinyldenes<sup>77</sup>.

In the present research the effects of a variety of substituents on the relative energies of singly and doubly substituted *trans* diphosphenes (RPPR) and *geminal* diphosphinyldene ( $\text{R}_2\text{PP}$ ) are studied. Isodesmic reaction schemes are utilized to derive insights concerning substituent effects, and natural bond order (NBO)<sup>43</sup> analyses were performed to investigate the nature of the bonding in these molecules.

## 2.2 Theoretical Methods

All computations were performed with the Q-CHEM 3.1 Program Suite<sup>84</sup>. For geometry optimization the def2-TZVPP basis of Weigend and Ahlrichs<sup>85</sup> was employed together with the B3LYP functional<sup>34</sup>. The stationary points were characterized by evaluating harmonic vibrational frequencies in order to identify structures as minima on the potential energy surfaces. Furthermore, isodesmic reaction schemes were employed in order to study substituent effects on the  $\text{P}=\text{P}$  moiety for both *geminal* (substituted diphosphinyldene) and *trans* (substituted diphosphene) isomers. Such isodesmic reactions have been extensively used to obtain accurate thermochemical predictions for many organic reactions<sup>86</sup>. The isodesmic reactions

used in this study are shown in Figure 2.1. The reaction energies were computed by taking the differences between the energies of reactants and products. Through these isodesmic relationships it is possible to examine the substituent effects for one (R1 and R2) and two (R3 and R4) substituents and shed light on whether there is a functional group that can substantially reduce the energy gap between the two isomers in question. Furthermore, the natural bond order (NBO)<sup>43</sup> method was used in order to obtain natural atomic charges and Wiberg bond orders<sup>87</sup> for the molecules under study.

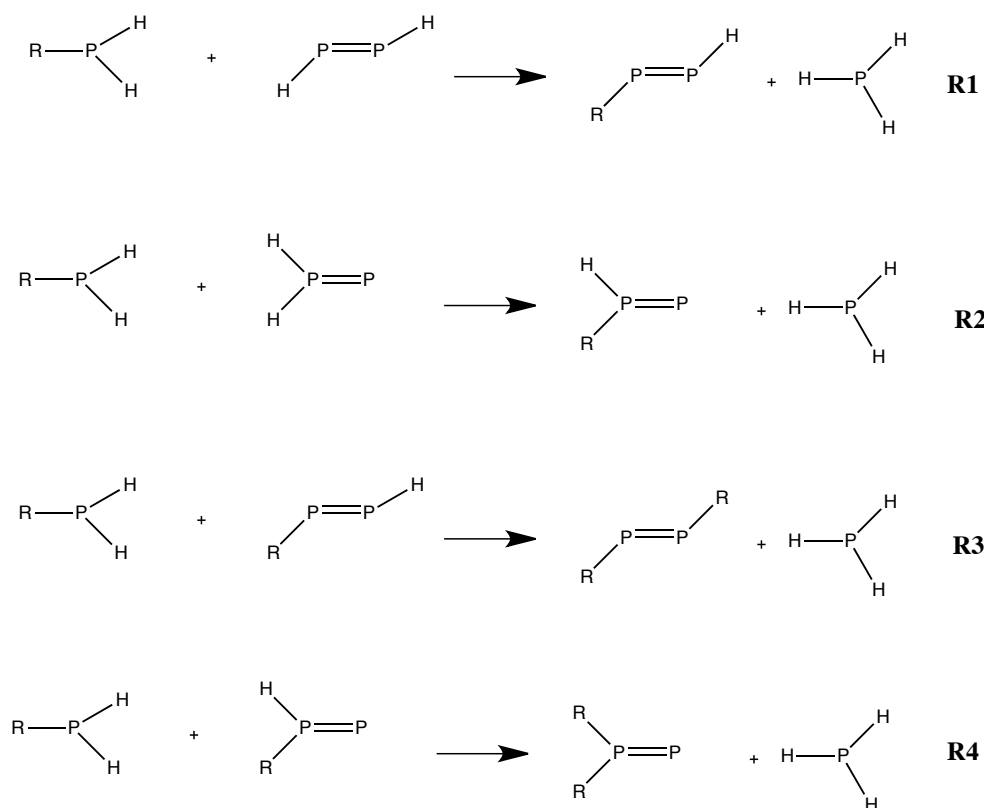


Figure 2.1: Isodesmic reactions for evaluating energetic effects related to the substitution of one or two hydrogens of diphosphene and diphosphylydene. Through these equations it is possible to separate the substituent effects on the two isomers, making it easier to study the energetics of single and double substitution.

## 2.3 Results and Discussion

### 2.3.1 Energetics

Figure 2.2 reports the ground state geometries for six of the 29 doubly substituted *geminal*-R<sub>2</sub>PP structures. Similarly, Figure 2.3 shows the geometries for six of the 29 doubly substituted *trans*-RPPR.

#### A. Energy Differences for Monosubstituted Systems

The first column in Table 2.1 shows the values for  $\Delta E_{sing}$ , which is the energy difference between RHPP and RPPH isomers, i.e.,  $\Delta E = E(\text{RHPP}) - E(\text{RPPH})$ . It can be seen that in all cases the monosubstituted RPPH is lower in energy than the RHPP isomer. However several substituents reduce the  $\Delta E_{sing}$  energy difference by approximately 4 kcal/mol from the parent H<sub>2</sub>PP-HPPH energy difference of 24.5 kcal/mol. The most effective functional group in reducing  $\Delta E_{sing}$  is lithoxy (OLi) with a  $\Delta E_{sing}$  of 10.5 kcal/mol. At the CCSD(T)/cc-pVTZ level of theory this energy difference between the two OLi substituted isomers increases to 13.5 kcal/mol. The least effective substituent, CN, has a  $\Delta E_{sing}$  value which is 3 kcal/mol higher than that of the parent hydrogen substituted compound. Of the five most effective substituents four are oxy groups, indicating that this general type of substituent is best for lowering the RHPP energy.

#### B. Energy Differences for Disubstituted Systems

The energy differences  $\Delta E_{doub}$  between the doubly substituted diphosphinylidene and diphosphene isomers  $\Delta E = E(\text{R}_2\text{PP}) - E(\text{HPPR})$  are given in the second column of Table 2.1. The only substituents capable of inverting the energy gap are OLi and ONa, where the C<sub>2v</sub> (OLi)<sub>2</sub>PP isomer lies 27.6 kcal/mol below the C<sub>i</sub> (OLi)PP(OLi) isomer. The best of the other substituents in reducing the energy gap are OH and OSiH<sub>3</sub> with R<sub>2</sub>PP-RPPR energy gaps of

4.5 and 5.4 kcal/mol respectively, such that the RPPR isomer is still moderately lower in energy.  $\text{OCH}_3$  and  $\text{NH}_2$  also perform well, as they reduce the energy difference by more than 15 kcal/mol. Due to the unusually large difference of over 30 kcal/mol between  $\text{OLi}$  and  $\text{ONa}$  and the next best substituent  $\text{OH}$ , both lithoxy substituted and diphosphinylidene and diphosphene isomers were reoptimized at the CCSD(T)/cc-pVTZ level of theory. The energy difference between  $(\text{OLi})_2\text{PP}$  and  $(\text{OLi})\text{PP}(\text{OLi})$  is predicted to be 33.0 kcal/mol which is 6 kcal/mol higher than the energy separation found at the B3LYP/def2-TZVPP level of theory, thus confirming the large energy difference favoring the diphosphinylidene isomer. A low lying triplet state for the  $(\text{OLi})\text{PP}(\text{OLi})$  isomer was also not found since the lowest triplet state lies 41.7 kcal/mol higher in energy than the singlet ground state. Another noteworthy substituent is the borane substituent  $\text{BH}_2$ . The geminal and trans isomers are second-order saddle points, however a minimum structure corresponding to a dibridged diphosphene is found on the potential energy surface. The good performance of  $\text{OLi}$ ,  $\text{ONa}$ ,  $\text{OH}$ ,  $\text{OSiH}_3$  and  $\text{OCH}_3$  indicates that functional groups which have electropositive atoms bonding to oxygen seem to be the best substituents for reducing the energy gap  $\Delta E_{\text{doub}}$ . Among the less effective substituents,  $\text{CN}$  is the worst with a  $\Delta E_{\text{doub}}$  of 32.0 kcal/mol, meaning that the energy difference between  $\text{R}_2\text{PP}$  and  $\text{RPPR}$  is increased by 7.5 kcal/mol with respect to the parent  $\text{P}_2\text{H}_2$  isomers.  $\text{NO}_2$  and the higher row halogens  $\text{Cl}$  and  $\text{Br}$  also increase the energy difference, thus further favoring the  $\text{RPPR}$  isomer. In general, all  $\pi$ -donating and  $\sigma$ -withdrawing groups significantly decrease the energy gap, with the exception of substituents containing a second row atom bonding to the phosphorus, where steric repulsion between the adjacent functional groups seems to disfavor the diphosphinylidene isomer. On the other hand  $\sigma$  and  $\pi$ -withdrawing functional groups like  $\text{CN}$  and  $\text{NO}_2$  are among the least effective substituents for reducing  $\Delta E_{\text{doub}}$ .

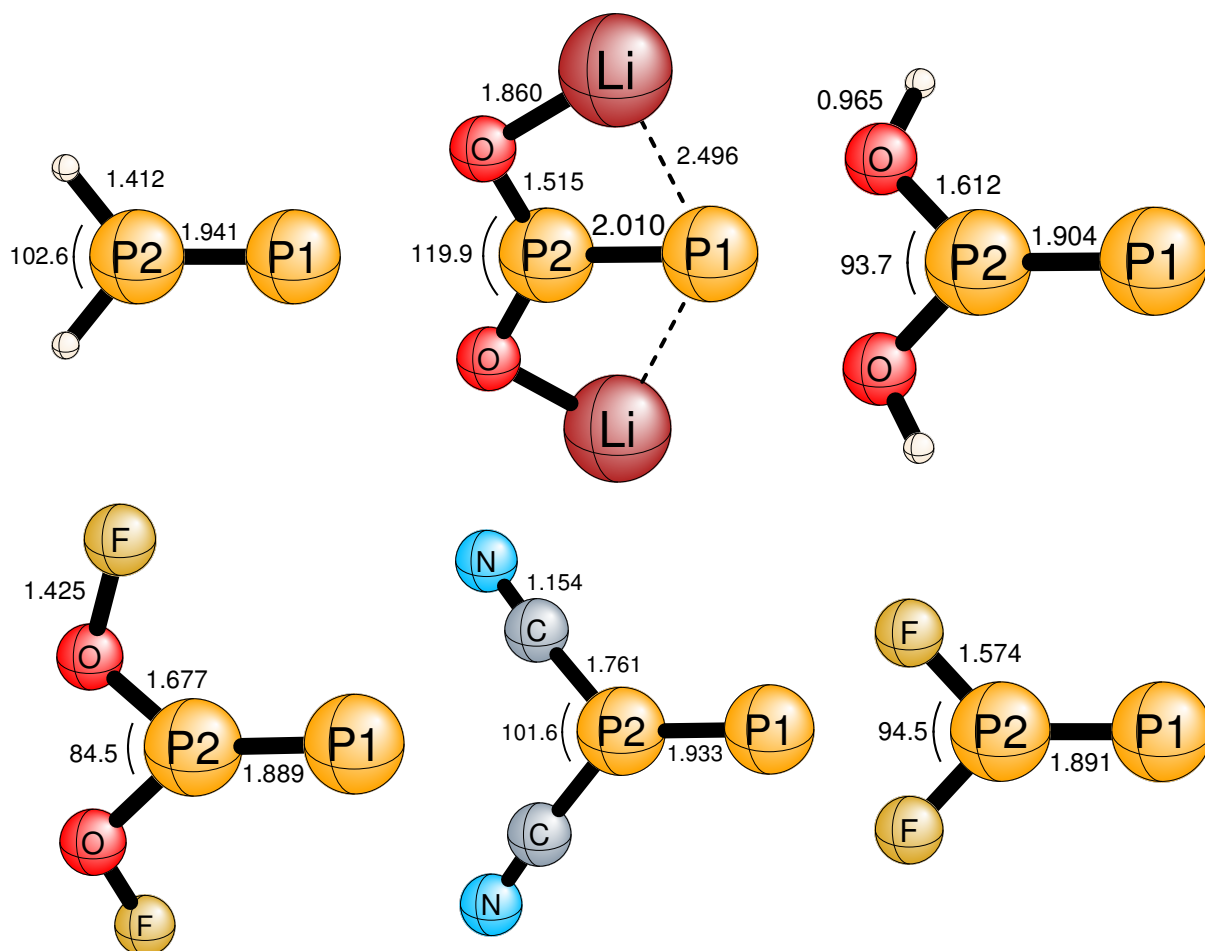


Figure 2.2: Theoretical geometries for representative diphosphinyldienes  $R_2PP$  with  $R = H$ , OLi, OH, OF, CN, F. Bond distances are reported in Å. As seen in Table 2 and 3, sixteen other structures with different substituents  $R$  were also studied

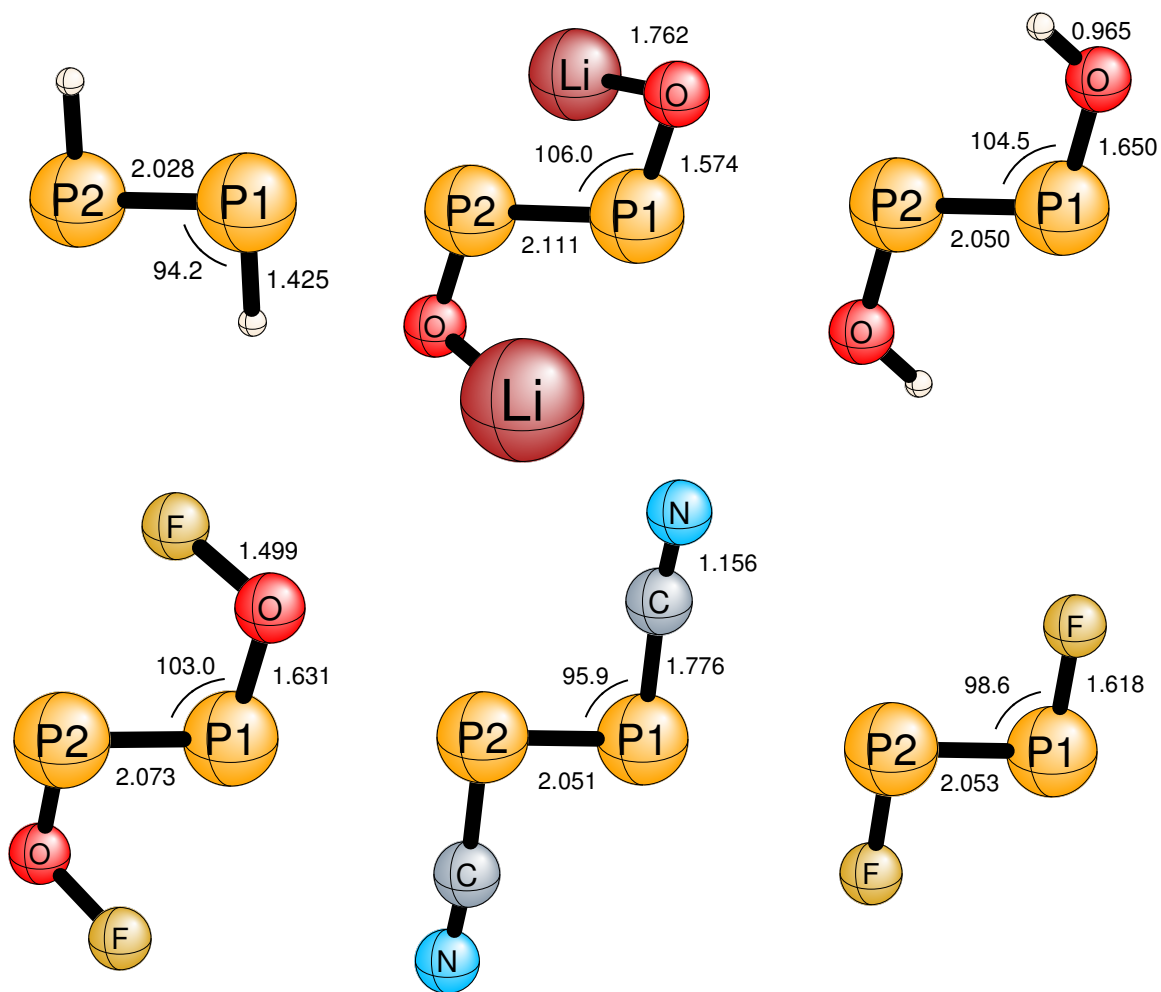


Figure 2.3: Theoretical geometries for representative diphosphenes RPPR with R = H, OLi, OH, OF, CN, F. Bond distances are reported in Å. As seen in Table 2 and 3, sixteen other structures with different substituents R were also studied



Table 2.1: Energy differences (kcal/mol) between the monosubstituted RHPP and RPPH isomers ( $\Delta E_{sing}$ ) and between disubstituted R<sub>2</sub>PP and RPPR ( $\Delta E_{doub}$ ).

$-R$	$\Delta E_{sing}$	$\Delta E_{doub}$
$-H$	24.5	24.5
$-CN$	27.5	32.0
$-OF$	23.9	27.1
$-C \equiv CH$	25.3	27.1
$-NO_2$	22.4	26.7
$-NF_2$	24.3	26.0
$-SiF_3$	25.7	25.9
$-Br$	22.9	25.8
$-CF_3$	24.3	25.3
$-Cl$	23.3	24.3
$-CH=O$	23.5	24.3
$-SH$	24.1	22.0
$-SiH_3$	23.0	21.6
$-PH_2$	22.7	21.3
$-BF_2$	22.0	20.4
$-Ph$	18.9	18.0
$-OOH$	22.4	19.1
$-CH_3$	20.1	15.9
$-N(CH_3)_2$	22.6	14.0
$-OBH_2$	21.0	13.1
$-ONH_2$	20.5	12.6
$-F$	20.6	12.1
$-NH_2$	23.0	8.8
$-OPh$	20.5	8.0
$-OCH_3$	17.9	6.6
$-OSiH_3$	18.4	5.4
$-OH$	18.2	4.5
$-ONa$	8.7	-27.0
$-OLi$	10.5	-27.6

### 2.3.2 Analysis from Isodesmic Reactions

In order to study in more detail the substituent effects on the P=P moiety for both diphosphinylidene and diphosphene isomers, the reaction energies of the following isodesmic reactions were obtained.



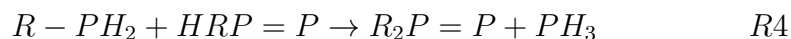
$$\Delta E(R1) = [E(R - PH_2) + E(HP = PH)] - [E(RP = PH) + E(PH_3)]$$



$$\Delta E(R2) = [E(R - PH_2) + E(H_2P = P)] - [E(HRP = P) + E(PH_3)]$$



$$\Delta E(R3) = [E(R - PH_2) + E(RP = PH)] - [E(RP = PR) + E(PH_3)]$$



$$\Delta E(R4) = [E(R - PH_2) + E(HRP = P)] - [E(R_2P = P) + E(PH_3)]$$

The reaction energies for mono-substitution [ $\Delta E(R1)$  and  $\Delta E(R2)$ ] and disubstitution [ $\Delta E(R3)$  and  $\Delta E(R4)$ ] are reported in Table 2.2 and Table 2.3, respectively. In the mono-substituted case (R1 and R2), a positive reaction energy indicates that the H<sub>2</sub>PP and HPPH reactants are preferred, such that replacement of one hydrogen by a substituent increases

the energy of the products. On the other hand, a negative reaction energy accounts for an energetically favorable effect upon the inclusion of a substituent to the P=P moiety, in the sense that the sum of the product energies is lower than the sum of the reactant energies. For the reactions leading to the disubstituted molecules (R3 and R4), a positive reaction energy favors the monosubstituted compound which now is on the reactant side of the reaction, whereas a negative reaction energy signals a preference for the disubstituted product side of the reaction. Thus, it is possible to analyze independently the energetics of the substituent effect of a functional group on H<sub>2</sub>PP, HPPH and RHPP, RPPH.

Upon the replacement of one hydrogen by a functional group in R1 and R2, most substituents yield negative isodesmic reaction energies for both isomers, meaning that both monosubstituted isomers are preferred relative to the parent H<sub>2</sub>PP and HPPH compound. However one can see that replacement of the hydrogen atom by substituent R is, in most cases, energetically more favorable for the RHPP [ $\Delta E(R2)$ ] than the RPPH [ $\Delta E(R1)$ ] conformation, since the latter yields a greater negative energy. The only exception to this trend is CN, where the monosubstituted RPPH conformation is favored upon substitution, whereas the substituted RHPP isomer gives a positive reactions energy, indicating an energetically less favorable configuration with respect to the parent diphosphinyldiene. This result is reflected in the value of  $\Delta E_{sing}$ , which is the energy difference between RHPP and RPPH. No particular diphosphinyldiene conformation is sufficiently lowered that  $\Delta E_{sing}$  remains close to the 24.5 kcal/mol of the parent molecules. Nonetheless, CH<sub>3</sub>, OH and especially OLi, reduce the energy difference by 5.6 kcal/mol, 6.3 kcal/mol, and 14.0 kcal/mol respectively, which represents some improvement.

Table 2.3 shows the reaction energies for the isodesmic reactions R3 and R4. In these reactions the remaining hydrogen is replaced by the second substituent, resulting in the disubsti-

tuted compound. For the substitution in the diphosphinyldiene isomer (R4) a trend similar to the replacement of the first hydrogen can be recognized. Most of the functional groups have a negative reaction energy  $\Delta E(R4)$  upon the inclusion of the second substituent. The isomers with the greatest substituent effects are OH (-12.6 kcal/mol),  $NH_2$  (-11.6 kcal/mol),  $OCH_3$  (-13.1 kcal/mol), and especially lithoxy OLi (-41.4 kcal/mol) and ONa (-43.1 kcal/mol). These reaction energies are only slightly lower than  $\Delta E(R2)$ , suggesting an additive substituent effect. The only substituent which presents a larger  $\Delta E(R4)$  than  $\Delta E(R2)$  is OLi where the reaction energy for the replacement of the second hydrogen increases by almost 5 kcal/mol. The picture is somehow different for the reaction energies of the diphosphene isomer ( $\Delta E(R3)$ ). The addition of a second substituent is only favorable for a few functional groups, whereas others even have a slightly positive reaction energy, meaning that they are energetically less favorable with respect to the monosubstituted compound. This suggests that the substitution by a second functional group does not contribute in lowering the energy of the disubstituted RPPR isomer, thus contrasting to the result found in the replacement of the first hydrogen. Figure 2.4 plots the relation between  $\Delta E_{doub}$  and  $\Delta E(R4)$ . A good correlation between these two energies can be appreciated, showing that an energetically more favorable substituent effect for the diphosphinyldiene than for the diphosphene isomer, upon the inclusion of the second substituent, seems to be responsible for the reduction of the energy gap. In order to explain the origin of the reduction of the energy difference between the  $R_2PP$  and RPPR isomer, the nature of the effect of adding a second substituent to the diphosphinyldiene isomer must be investigated.

Table 2.2: Isodesmic reaction energies (kcal/mol) for the singly substituted diphosphenes and diphosphenylidenes:

$-R$	$\Delta E(R1)$	$\Delta E(R2)$
$-H$	0.0	0.0
$-CN$	-2.3	0.7
$-OF$	-7.9	-8.5
$-C \equiv CH$	-4.2	-3.4
$-NO_2$	-2.5	-4.5
$-NF_2$	-2.4	-2.5
$-SiF_3$	1.4	2.7
$-Br$	-5.9	-7.4
$-CF_3$	0.5	0.3
$-Cl$	-6.6	-7.8
$-CH=O$	-1.0	-2.0
$-SH$	-6.4	-6.8
$-SiH_3$	-0.2	-1.6
$-PH_2$	-2.3	-4.1
$-BF_2$	2.3	-0.2
$-Ph$	-3.9	-9.5
$-OOH$	-8.7	-10.8
$-CH_3$	-2.0	-6.4
$-N(CH_3)_2$	-12.7	-14.6
$-OBH_2$	-7.4	-11.0
$-ONH_2$	-9.7	-13.7
$-F$	-7.9	-11.8
$-NH_2$	-10.8	-12.3
$-OPh$	-8.6	-12.6
$-OCH_3$	-9.8	-16.7
$-OSiH_3$	-9.2	-15.2
$-OH$	-9.1	-15.3
$-ONa$	-26.8	-42.6
$-OLi$	-22.5	-36.5

Table 2.3: Isodesmic reaction energies (kcal/mol) for the doubly substituted diphosphenes and diphosphenylidenes:

$-R$	$\Delta E(R3)$	$\Delta E(R4)$
$-H$	0.0	0.0
$-CN$	0.3	4.9
$-OF$	-2.4	0.8
$-C \equiv CH$	-3.8	-2.0
$-NO_2$	3.1	7.4
$-NF_2$	3.6	5.3
$-SiF_3$	3.1	3.3
$-Br$	-3.9	-1.1
$-CF_3$	3.1	4.1
$-Cl$	-2.6	-1.5
$-CH = O$	1.2	0.5
$-SH$	-0.8	-2.8
$-SiH_3$	-1.1	-1.5
$-PH_2$	-2.3	-3.7
$-BF_2$	2.9	1.26
$-Ph$	-2.2	-3.3
$-OOH$	-2.8	-4.7
$-CH_3$	-2.0	-5.3
$-N(CH_3)_2$	2.2	-6.4
$-OBH_2$	0.8	-6.9
$-ONH_2$	-0.4	-8.3
$-F$	2.5	-6.1
$-NH_2$	2.7	-11.6
$-OPh$	2.9	-9.6
$-OCH_3$	-1.8	-13.1
$-OSiH_3$	0.4	-12.6
$-OH$	1.1	-12.6
$-ONa$	-7.4	-43.1
$-OLi$	-3.3	-41.4

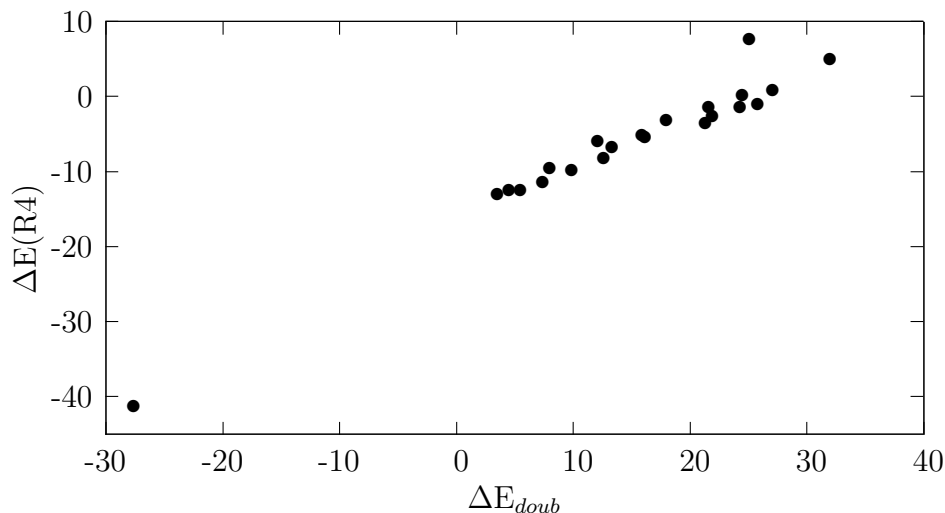


Figure 2.4: Plot of the doubly (doub) substituted diphosphinylidene-diphosphene energy gap  $\Delta E_{doub} = E(R_2P=P) - E(RP=PR)$  against the reaction energies for isodesmic reaction R4  $R - PH_2 + HRP = P \rightarrow R_2P = P + PH_3$ . The good correlation between  $\Delta E(R4)$  and  $\Delta E_{doub}$  indicates that the reduction of the energy difference between diphosphene and diphosphinylidene isomers is mainly due to a favorable substituent effect after the incorporation of the second substituent into the parent diphosphinylidene compound.

### 2.3.3 Analysis of the Bonding

In order to get more insight into the electronic effects responsible for reducing the energy gap between RPPR and  $R_2PP$  isomers, NBO analysis was performed. Wiberg bond orders were obtained for all disubstituted diphosphenyliidene and diphosphene isomers and are shown in Table 2.4. For the  $R_2PP$  conformation the substituent yielding the highest P=P bond order is fluorine with a bond order of 2.50. Jin et al. attributed this to negative hyperconjugation of the in-plane lone pair on the terminal phosphorous atom with low lying P-F  $\sigma^*$  orbitals<sup>79</sup>. The NBO analysis confirms this assumption, since it renders a third partial phosphorus-phosphorus bond which is polarized toward the terminal phosphorous atom with a natural orbital occupation of 1.87. Such a partial triple bond is found for several other

substituents which have an electronegative atom attached to the P=P moiety. Moreover, the relatively short P-P bond length in these isomers also suggests the presence of a partial P-P triple bond. However this does not seem to be the energetic effect responsible for the decrease of the RPPR-R<sub>2</sub>PP energy gap, since the substituents NO<sub>2</sub> (2.39) and OH (2.40) yield almost the same bond order and almost identical bond distances, while having very different R<sub>2</sub>PP-RPPR energy gaps (25.1 kcal/mol for NO<sub>2</sub> vs 4.5 kcal/mol for OH). Also, OLi, the only substituent which inverts the energy order, has the lowest phosphorus-phosphorus bond order (1.77) and the longest P-P bond length (2.010 Å) of all, suggesting that there is another energetically more significant effect than negative hyperconjugation of the in-plane phosphorous lone pair.

For the *trans*-RPPR isomers the picture is somewhat different. The parent diphosphene has a well localized P=P bond with a bond order of 2.03, while all other substituted compounds have lower bond orders. This is especially the case for substituents with an out-of-plane lone pair, due to delocalization of that lone pair into P-P  $\pi^*$ . Since in the RPPR isomer there is no possible negative hyperconjugation of an in-plane lone pair to form a third bond, as in the R<sub>2</sub>PP case, the resulting bond order is lowered. It is noteworthy that this is the inverse effect to that found for the R<sub>2</sub>PP isomers, where most substituents increase the bond order of the P-P bond. Electrostatic effects also seem to be important in weakening the P-P bond, since the adjacent phosphorus atoms have the same charge upon substitution, resulting in repulsion and an increase in the P-P bond distance and hence a weaker  $\pi$ -bond.

Table 2.5 shows the atomic charges for the doubly and singly (in parentheses) substituted R<sub>2</sub>PP, RHPP and RPPR, RPPH isomers. In the parent H<sub>2</sub>PP isomer the terminal phosphorus possesses a negative charge while the phosphorus atom bonded to the substituents has a positive charge. When comparing the singly substituted RHPP with the singly substituted



RPPH isomers, good agreement between the atomic charges can be found. Substitution by a more electronegative functional group increases, in both isomers, the positive charge on phosphorus P2 which is bonded to that functional group, while the substitution of a more electropositive compound yields a negative charge on P2, as expected. The remaining hydrogen does not seem to play a preponderant role, since the charges on both isomers are fairly similar.

When comparing the singly with the doubly substituted diphosphinylidene isomers some noticeable changes can be appreciated. The charge on both substituents in the disubstituted isomer is of the same magnitude as that for the monosubstituted compound, indicating the absence of a saturation effect on the ability to withdraw electron density from the phosphorus. Furthermore the charge on P2 nearly doubles compared to the singly substituted case, thus gaining a significant positive charge. This generates a very favorable electrostatic interaction in the diphosphinylidene case, which is accentuated by electronegative substituents like  $\text{NH}_2$ ,  $\text{OH}$  and  $\text{F}$ . This finding is in good agreement with the isodesmic reaction energies, since these substituents have significant negative reaction energies for the second substitution. For the electropositive  $\text{SiH}_3$ , the phosphorus atom forming bonds to the substituents has a negative charge, whereas the charge on silicon is positive, showing the same trend with opposing polarity as with the electronegative substituents.

In the case of the two substituents which energetically favour the diphosphinylidene structure ( $\text{OLi}$ ,  $\text{ONa}$ ) a significant charge separation can be appreciated where atom P1 almost doubles its negative charge (-1.11), whereas P2 acquires a significant positive charge (1.60) after replacing the second hydrogen on P2. Furthermore, the negative charge on the atom bonded to phosphorus is the same as in the singly substituted case for both atoms. This charge separation, induced by geminal substitution, creates a strong and favorable diphosphinylidene isomer coulombic interaction that is not present in the diphosphene isomer.

The destabilization of the diphosphene isomer with the substitution of the second hydrogen can also be rationalized, as mentioned before, in terms of unfavorable charge distribution that puts positive charge on adjacent phosphorous atoms. These interactions seem to be responsible for the reduction and inversion of the energy gap between both. This becomes especially evident when looking at the hydroxyl derived substituents OF, OH and OLi, where the energy gap decreases as the electropositive character of the atom bonded to the oxygen increases. Additionally, the positively charged Li can further interact with the negatively charged terminal phosphorus, providing additional energetic stabilization to this isomer and thus successfully inverting the energy gap between diphosphinylidene and diphosphene isomers.

Table 2.4: Wiberg bond orders for R<sub>2</sub>PP and RPPR structures.

$-R$	R <sub>2</sub> PP	RPPR
$-H$	2.14	2.03
$-CN$	2.05	1.78
$-OF$	2.33	1.78
$-C \equiv CH$	2.03	1.72
$-NO_2$	2.39	1.90
$-NF_2$	2.35	1.83
$-SiF_3$	2.45	1.98
$-Br$	2.29	1.88
$-CF_3$	2.22	1.96
$-Cl$	2.32	1.86
$-CH = O$	1.98	1.83
$-SH$	2.22	1.81
$-SiH_3$	1.95	1.96
$-PH_2$	2.13	1.90
$-BF_2$	1.82	1.92
$-Ph$	2.11	1.81
$-OOH$	2.38	1.79
$-CH_3$	2.20	1.93
$-OBH_2$	2.42	1.86
$-ONH_2$	2.37	1.81
$-F$	2.51	1.89
$-N(CH_3)_2$	2.24	1.68
$-OPh$	2.41	1.82
$-NH_2$	2.37	1.81
$-OCH_3$	2.36	1.80
$-OSiH_3$	2.36	1.84
$-OH$	2.40	1.83
$-ONa$	1.68	1.62
$-OLi$	1.77	1.62

Table 2.5: Natural atomic charges from NPA for the doubly substituted isomers. In parentheses are the charges for the singly substituted isomer.

-R	<i>diphosphinylidene</i>				<i>diphosphene</i>			
	P1	P2	H		P1	P2	H	
-H	-0.12	0.16	-0.02		0.04	0.04	-0.04	
-F	P1 -0.25 (-0.16)	P2 1.32 (0.74)	F -0.54 (-0.56)		P1 0.56 (-0.097)	P2 0.56 (0.68)	F 0.56 (-0.56)	
-NH <sub>2</sub>	P1 -0.39 (-0.28)	P2 1.11 (0.67)	N -1.16 (-1.14)	H(N) 0.40 (0.40)	P1 0.35 (-0.21)	P2 0.35 (0.55)	N -1.13 (-1.12)	H(N) 0.39 (0.39)
-CN	P1 0.06 (-0.03)	P2 0.55 (0.36)	C -0.11 (-0.11)	N -0.19(-0.23)	P1 0.37 (0.11)	P2 0.37 (0.29)	C -0.14 (-0.11)	N -0.24 (-0.27)
-CH <sub>3</sub>	P1 -0.22 (-0.18)	P2 0.71 (0.44)	C -0.95 (-0.94)	H(C) 0. 23 (0.24)	P1 0.25 (-0.03)	P2 0.25 (0.31)	C -0.92 (-0.94)	H(C) 0.22 (0.23)
-SiH <sub>3</sub>	P1 -0.09 (-0.05)	P2 -0.27 (-0.11)	Si 0.61 (0.61)	H(Si) -0.14 (-0.14)	P1 -0.12 (0.05)	P2 -0.12 (-0.13)	Si 0.57 (0.55)	H(Si) -0.14 (-0.14)
-OF	P1 -0.13 (-0.13)	P2 1.19 (0.63)	O -0.45 (-0.37)	F -0.16 (-0.12)	P1 0.52 (-0.01)	P2 0.54 (-0.07)	O -0.38 (0.62)	F -1.16 (-0.38)
-OSiH <sub>3</sub>	P1 -0.37 (-0.23)	P2 1.33 (0.76)	O -1.12 (-1.12)	Si 1.21 (1.21)	P1 0.51 (-0.10)	P2 0.51 (0.64)	O -1.12 (-1.13)	Si 1.21 (1.23)
-OH	P1 -0.39 (-0.24)	P2 1.27 (0.73)	O -0.94 (-0.95)	H(O) 0.51 (0.51)	P1 0.46 (-0.11)	P2 0.46 (0.60)	O -0.94 (-0.95)	H(O) 0.48 (0.49)
-OCH <sub>3</sub>	P1 -0.41 (-0.27)	P2 1.30 (0.75)	O -0.76 (-0.76)	C -0.24 (-0.25)	P1 0.47 (-0.12)	P2 0.47 (0.61)	O -0.75 (-0.76)	C -0.25 (-0.24)
-OLi	P1 -1.11 (-0.58)	P2 1.60 (0.91)	O -1.17 (-1.17)	Li 0.92(0.89)	P1 0.33 (-0.53)	P2 0.33 (0.80)	O -1.12 (-1.92)	Li 0.88 (0.90)

## 2.4 Conclusions

Theoretical methods have been employed in order to obtain the energy separation between substituted singlet diphosphenes ( $R_2PP$ ) and diphosphinylienes ( $RPPR$ ). Among  $R$  groups considered here the only substituents capable of inverting the energetic ordering between both isomers are lithoxy ( $OLi$ ) and  $ONa$ , while a several others (e.g.  $OCH_3$ ) reduce the gap quite substantially.

Natural charge analysis helps to elucidate how the second substituent on the  $R_2PP$  isomer lowers its energy with respect to the  $RPPR$  isomer. It is found that a very favorable coulombic interaction is present in the diphosphinylidene structure  $(OLi)_2PP$  but not in the  $(OLi)PP(OLi)$  diphosphene isomer.

## 2.5 Acknowledgments

This research was supported by the National Science Foundation Grant CHE-1054286. We thank Dr. Andrew Simmonett and Mr. Alexander Sokolov for many helpful discussions.

# Chapter 3

## Structure, Bonding and Aromaticity of $\text{Ge}_2\text{CH}_2$

a

### 3.1 Introduction

The chemistry of germanium is rapidly developing. It is now widely realized that germanium can form stable compounds in the divalent (carbene-like) as well as the expected tetravalent state and exhibits a variety of binding motifs.<sup>88</sup> Species with multiple bonds to germanium have been reported<sup>88–90</sup>. Furthermore, germanium has been shown to form strained three- and four-membered rings<sup>88,89</sup>, including aromatic molecules with two and six  $\pi$ -electrons<sup>91–94</sup>.

Among the simplest divalent species, compounds  $\text{Ge}_n\text{C}_{3-n}\text{H}_2$  ( $n = 1 - 3$ ) are of particular interest<sup>95</sup>. These molecules are valence isoelectronic to cyclopropenylidene ( $\text{C}_3\text{H}_2$ ) and its silicon derivatives ( $\text{SiC}_2\text{H}_2$  and  $\text{Si}_2\text{CH}_2$ ), which have drawn much attention due to their unique reactivity and primal role in the chemistry of the interstellar medium<sup>96,97</sup>. Several

---

<sup>a</sup>S. Vogt-Geisse, A. Y. Sokolov, S. R. McNew, Y. Yamaguchi, H.F. Schaefer, submitted to the J. Phys. Chem. A. Reprinted here with the permission of the American Chemical Society

experimental and theoretical studies have been carried out to determine the structures of the  $C_3H_2$  isomers<sup>98–105</sup> and its silicon analogues<sup>106–118</sup>. The two lowest-energy structures located on the singlet potential energy surface (PES), of  $C_3H_2$  are the cyclic isomer  $:C(CH)_2$  followed by the propadienylidene structure  $:C=C=CH_2$ <sup>104</sup> (Scheme Scheme 3.1). The lowest energy triplet structure was found to lie close in energy to propadienylidene<sup>105</sup>. Interestingly, the ground state of  $C_3H_2$  is isoelectronic to the deprotonated cyclopropenium ion  $[C_3H_3]^+$  with two  $\pi$ -electrons and can therefore be considered the smallest aromatic carbene.

In 1986 Frenking *et al.*<sup>106</sup> investigated structural isomers of  $SiC_2H_2$  at the Hartree-Fock (HF) and the configuration interaction with singles and double excitations (CISD) levels of theory. They found that singlet 1-silacyclopropenylidene ( $:Si(CH)_2$ ) was the lowest energy structure (Scheme Scheme 3.1). Matrix isolation infrared (IR) spectroscopy experiments performed by Maier and co-workers<sup>107–109</sup> detected four different isomers of  $SiC_2H_2$ . The cyclic  $:Si(CH)_2$  was confirmed to be the global minimum. More recent high accuracy *ab initio* studies employing the coupled cluster (CC) theory methods supported the previous experimental and theoretical results about the energetic ordering of various  $SiC_2H_2$  isomers<sup>110–114</sup>. The geometric and electronic structure of  $Si_2CH_2$  is fundamentally different from that of  $C_3H_2$  and  $SiC_2H_2$ .  $Si_2CH_2$  was first studied by Jemmis *et al.*<sup>115</sup> using the second order Møller-Plesset (MP2) method. Jemmis found an unusual hydrogen-bridged cyclic structure  $(Si \cdots H \cdots Si)(CH)$  with three-center two-electron  $Si \cdots H \cdots Si$  bond to have the lowest energy (Scheme Scheme 3.1). This peculiar result was confirmed by the latest studies employing CC theory and the focal point extrapolation technique.<sup>116,117</sup> Recently, the paper by Lu and co-workers presented an anharmonic rovibrational analysis of the global minimum structure of  $Si_2CH_2$ .<sup>118</sup>

The isovalent germanium species  $Ge_nC_{3-n}H_2$  ( $n = 1 - 3$ ) have been investigated to a much lesser extent than the corresponding silicon compounds. The  $Ge(C_2H_2)$  complex was produced by laser ablation and detected by matrix isolation IR spectroscopy.<sup>119</sup> Two structural

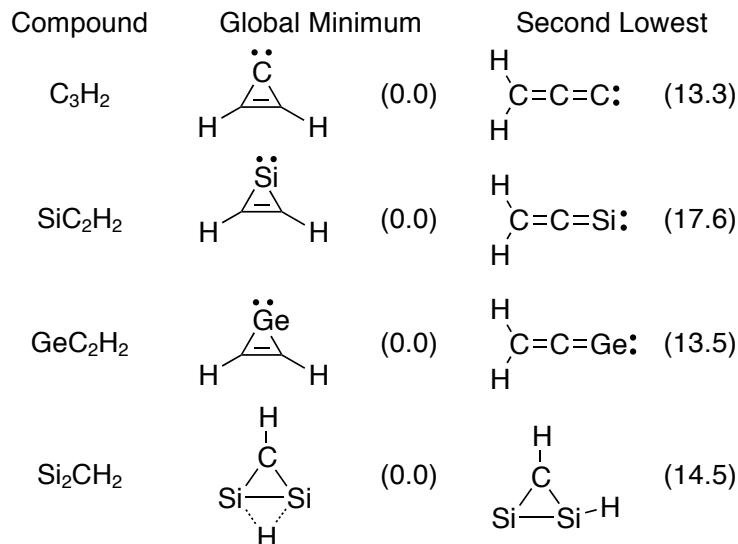
isomers were characterized: cyclic germylene  $:\text{Ge}(\text{CH})_2$  isomer (1-germacyclopropenylidene, Scheme Scheme 3.1) and bent ethynylgermylene. The magnitude of the C–C stretching vibrational frequency in the cyclic isomer indicated that its structure is similar to that of  $\text{C}_3\text{H}_2$ , as opposed to the metal–acetylene  $\pi$ -complex. A very recent theoretical study of  $\text{GeC}_2\text{H}_2$  structures and energetics using the coupled cluster methods located a total of nine different structural isomers on the singlet PES and assigned the cyclic  $:\text{Ge}(\text{CH})_2$  isomer to be the global minimum (in Scheme Scheme 3.1).<sup>120</sup> The computed C–C stretching harmonic vibrational frequency of the cyclic isomer was found to be in very good agreement with the experiment<sup>119</sup>.

To our knowledge, nothing is known about the  $\text{Ge}_2\text{CH}_2$  species from the literature. Using high accuracy coupled cluster methods we aim to predict geometric structures, relative energies, harmonic vibrational frequencies and associated infrared (IR) intensities of various  $\text{Ge}_2\text{CH}_2$  isomers. Eleven stationary points were identified on the  $\text{Ge}_2\text{CH}_2$  PES. Among these there are two isomers with very unusual bonding patterns: **1S** is a hydrogen-bridged structure and **3S** possesses a tetravalent planar carbon. The electronic structure of the lowest energy isomers will be analyzed using natural bond orbital (NBO) methods to provide insights about the nature of chemical bonds in digermanium compounds with unusual bonding motifs.

## 3.2 Theoretical Procedures

A stochastic search using the kick procedure developed by Saunders<sup>121–123</sup> was utilized, in order to systematically search for stationary points on the potential energy surface (PES). The initial geometries for optimization were generated by randomly displacing the atoms from a starting position in which all atoms fall on the same point in space. For the sake





Scheme 3.1: Two lowest energy isomers of  $XC_2H_2$  ( $X = C, Si, Ge$ ) and  $Si_2CH_2$ . The theoretical energies (in  $\text{kcal mol}^{-1}$ ) relative to the corresponding global minimum structures are given in parentheses. The relative energies are taken from Refs. 105 ( $C_3H_2$ ), 114 ( $SiC_2H_2$ ), 120 ( $GeC_2H_2$ ) and 117 ( $Si_2CH_2$ ).

of minimizing computational effort three conditions were applied, which the displaced geometries had to comply with in order to be optimized: 1) No atom could be kicked farther than 4.5 Å from its initial position, 2) the minimal distance between any two atoms has to be greater than 1.0 Å, and 3) the maximal distance between any two atoms should not be greater than 6.0 Å. Five hundred structures that met these requirements were generated and optimized with the B3LYP/6-31G method, using the QCHEM quantum chemistry software package<sup>124</sup>. Of the 500 structures the optimization procedure was successful in 154 cases which were distributed among 7 minima on the PES.

The optimization was refined using the correlation-consistent polarized valence basis sets cc-pVXZ ( $X = D, T, \text{ and } Q$ ) developed by Dunning and co-workers<sup>24,25</sup>. Zeroth-order descriptions of all stationary points were obtained using the closed-shell restricted Hartree-Fock (RHF) self-consistent field (SCF) method. Dynamic correlation effects were included

using the coupled cluster (CC) method with single, double excitations (CCSD)<sup>14,15</sup> and CCSD with perturbative triple [CCSD(T)]<sup>125–127</sup>, full triple and perturbative quadruple. The total of 19 lowest lying core orbitals were kept frozen in the correlated wavefunctions corresponding to atomic orbitals (AO) 1s, 2s, 2p, 3s, and 3p of germanium and the 1s-AO of carbon.

The nature of the molecular wavefunction of each stationary point was analyzed using the complete active space self-consistent field method (CASSCF)<sup>128,129</sup> with the cc-pVQZ basis set at the CCSD(T)/cc-pVQZ optimized geometries. The active space was chosen to be 10 electrons in 9 molecular orbitals (MOs). For the representation of the CASSCF wavefunctions the reduced one-particle density matrix was diagonalized to obtain the natural orbitals and occupation numbers.<sup>130</sup>

The relative energies of eleven different Ge<sub>2</sub>CH<sub>2</sub> stationary points with respect to the global minimum (**1S**) were obtained using the focal point analysis technique (FPA)<sup>20–23</sup>. In this technique, energy values obtained at the SCF, MP2, CCSD, CCSD(T), coupled cluster with singles, doubles, and triples (CCSDT) and perturbative quadruple excitations CCSDT(Q)<sup>131,132</sup> levels of theory with the cc-pVXZ basis sets were used to obtain relative energies extrapolated to the complete basis set (CBS) limit. The geometries employed in the focal point analysis (FPA) were optimized at the CCSD(T)/cc-pVQZ level of theory. In the FPA the total energy was extrapolated to the complete basis set limit (CBS) using the functional form<sup>133,134</sup>

$$E_{SCF}(X) = A + Be^{-CX} \quad E_{CORR} = E + FX^{-3}$$

where  $E_{SCF}$  and  $E_{CORR}$  are the extrapolated SCF and correlation energies and, and  $X$  is the cardinal number corresponding to the maximum angular momentum of the basis set.  $A$ ,  $B$ ,  $C$  and  $E$ ,  $F$  are fitting parameters for the SCF and correlation energies respectively.

Core correlation ( $\Delta E_{core}$ ) effects were computed as the difference between frozen-core and all-electron CCSD(T)/cc-pCVQZ energies. The non-diagonal contribution to the Born-

Oppenheimer energy ( $\Delta E_{DBOC}$ ) was accounted for via the diagonal Born-Oppenheimer correction (DBOC), at the CCSD(T)/cc-pVTZ level of theory. Finally, special relativity effects ( $\Delta E_{rel}$ ) were accounted for by the application of the mass-velocity and Darwin one-electron terms computed at CCSD(T)/cc-pVQZ level of theory.

The structures of the  $\text{Ge}_2\text{CH}_2$  isomers were optimized using analytic derivative methods. Harmonic vibrational frequencies were also analyzed analytically. The harmonic vibrational frequencies were used to characterize the nature of each stationary point on the  $\text{Ge}_2\text{CH}_2$  PES. Electronic structure computations were carried out using CFOUR<sup>135</sup> and MOLPRO<sup>136</sup> quantum chemistry software packages. In order to analyze bonding different bonding patterns among the isomers, the natural bond orbital (NBO)<sup>43</sup> method. The reported orbital hybridization and occupations were obtained using this method. Finally, Nuclear independent chemical shifts (NICS)<sup>137,138</sup> were computed at the PW91/def2-TZVPP level of theory. The total NICS value was obtained at the center of the ring [NICS(0)]. Additionally, the dissected canonical orbital NICS(0) <sub>$\pi_{zz}$</sub>  was computed. The NICS(0) <sub>$\pi_{zz}$</sub>  extracts the out-of-plane tensor component of the isotropic NICS and includes only the aromaticity contribution from the  $\pi$  MOs. This index has been found to be the best indicator for  $\pi$  aromaticity<sup>139</sup>.

### 3.3 Results and Discussion

Figure 3.1 to Figure 3.5 show the optimized structures of eleven stationary points located on the  $\text{Ge}_2\text{CH}_2$  singlet ground state PES at the CCSD(T)/cc-pVQZ level of theory. Among these seven structures are minima (**1S** – **7S**), two are transition states (**TS1** and **TS2**), and two are stationary points of Hessian index 2 (**SSP1** and **SSP2**). Three lowest energy structures **1S**–**3S** are cyclic (shown in Figure 3.1 to Figure 3.3). Structures **4S** - **6S** are open-chain with linear (**4S** and **5S**) and bent (**6S**)  $\{\text{Ge}_2\text{C}\}$  fragments (shown in Figure 3.4) Focal point analyses (FPA) of the relative energies between isomers **1S**, **2S** and **3S** are provided in Table 1 and Table 2, respectively. For the remaining stationary points the relative energies from FPA are given in Tables S1 – S8. The final energies (with the ZPVE, core, DBOC, and relativistic corrections) for the eleven stationary points located on the singlet PES are presented in Table 3. The triplet states of the low-energy structures are more than 30 kcal mol<sup>-1</sup> higher in energy than the corresponding singlet states and, therefore will not be discussed in this paper.

#### 3.3.1 Relative Energies and CASSCF Wave Functions

The nature of the molecular wavefunctions was analyzed using the CASSCF method with the cc-pVQZ basis set. For each of the stationary points the wavefunction has a dominant contribution from a single electronic (reference) configuration.

##### Global Minimum **1S**

The ground electronic configuration of the unconventional  $C_{2v}$  symmetry global minimum structure **1S** (in Figure 3.1) is mainly described as:

$$\Phi_1 = [\text{core}]12a_1^2 13a_1^2 11b_2^2 14a_1^2 15a_1^2 12b_2^2 5b_1^2 \quad |CI|^2 = 0.90,$$

where [core] denotes the 29 low-lying doubly occupied MOs (including the 3d orbitals of Ge) and  $|CI|^2$  is the square of the corresponding configuration interaction (CI) coefficient. The next two doubly excited configuration state functions (CSFs) are  $\Phi_2[5b_1^2 \rightarrow 6b_1^2]$  ( $|CI|^2 = 0.01$ ) and  $\Phi_3[5b_1^2 \rightarrow 5a_2^2]$  ( $|CI|^2 < 0.01$ ). As one can see in Figure 3.1, these excitations correspond to the electronic transitions from the bonding  $\pi$ -type  $5b_1$  orbital to the antibonding  $\pi^*$ -type  $6b_1$  ( $\pi \rightarrow \pi^*$  transition) and non-bonding  $5a_2$  orbitals.

## **2S and 3S ( Figure 3.2 and Figure 3.3 and Table 3.1 and Table 3.2)**

The electronic configuration of structures **2S** and **3S** ( $C_s$  symmetry, in Figure 3.2 and Figure 3.3) is:

$$\Phi_1 = [\text{core}]22a'^2 23a'^2 24a'^2 25a'^2 26a'^2 9a''^2 27a'^2 \quad |CI|^2 = 0.90 \text{ (2S)} \text{ and } 0.89 \text{ (3S)}$$

The other two important CSFs are  $\Phi_2[9a''^2 \rightarrow 10a''^2]$  ( $|CI|^2 = 0.01$  (**2S**),  $0.03$  (**3S**)) and  $\Phi_3[27a'^2 \rightarrow 28a'^2]$  ( $|CI|^2 < 0.01$  (**2S**, **3S**)). The former CSF corresponds to the  $\pi \rightarrow \pi^*$  transition, whereas the latter describes a transition within the in-plane  $\sigma$ -orbital framework, as shown in Figure 3.2 and Figure 3.3.

As may be seen from Table 3.1, the **2S** isomer is found to lie  $17.7 \text{ kcal mol}^{-1}$  higher in energy than the global minimum **1S**. At the SCF/cc-pVQZ level of theory the energy difference between these two isomers is  $18.3 \text{ kcal mol}^{-1}$  which is only  $0.5 \text{ kcal mol}^{-1}$  higher than the energy obtained at the CCSDT(Q)/CBS, showing that the inclusion of correlation treatment has only little effect on this particular energy difference.

The focal point analysis (FPA) for the energy difference between isomers **1S** and **3S** is

presented in Table Table 3.2. The energy separation is predicted to be 18.0 kcal mol<sup>-1</sup>. The inclusion of correlation effects seem to play a more preponderant role for this isomer since it decreases the energy from 21.9 kcal mol<sup>-1</sup> at the SCF/CBS level to 18.0 kcal mol<sup>-1</sup> for the final extrapolated result. This can also be appreciated when looking at the MP2 energy contribution  $\delta(\text{MP2})$  increments in Table 3.1 and Table 3.2. While the MP2 correction to the relative energy at CBS is minimal (-0.09 kcal mol<sup>-1</sup>) for the **2S** isomer, for **3S**, the same quantity amounts to -4.36 kcal mol<sup>-1</sup>. The same trend holds using higher level correlated methods (CCSD, CCSD(T)), meaning that correlation effects are more significant in **3S** than in the **2S** isomer. The total correction from correlation energy in the **3S** isomer amounts to 3.85 kcal mol<sup>-1</sup> while, in **2S** it is only 0.55 kcal mol<sup>-1</sup>. After including the ZPVE, DBOC, core and relativistic corrections the energy difference between **1S** and **2S** amounts to 17.23 kcal mol<sup>-1</sup>. The energy gap between **1S** and **3S** is 18.31 kcal mol<sup>-1</sup>.

#### 4S and 5S (Figure 3.4 and Tables A.1 and A.2)

The wavefunctions of the non-cyclic  $C_{2v}$  symmetry isomers **4S** and **5S** (in Figure 3.4) are dominated by the following CSF:

$$\Phi_1 = [\text{core}]16a_1^2 17a_1^2 7b_2^2 18a_1^2 19a_1^2 7b_1^2 8b_2^2 \quad |CI|^2 = 0.85 \text{ (4S)} \text{ and } 0.92 \text{ (5S)}.$$

The other two CSFs with significant contributions are  $\Phi_2[8b_2^2 \longrightarrow 9b_2^2]$  ( $|CI|^2 = 0.05$  for **4S** and  $|CI|^2 = 0.02$  for **5S**) and  $\Phi_3[7b_1^2 \longrightarrow 8b_1^2]$  ( $|CI|^2 = 0.03$  for **4S** and  $|CI|^2 = 0.01$  for **5S**). These excitations correspond to  $\pi \rightarrow \pi^*$  transitions in and out of the molecular plane, respectively. The relative energies of **4S** and **5S** with respect to the global minimum are 30.9 and 40.5 kcal mol<sup>-1</sup> (Table 3.3).

### 6S (in Figure 3.4 and in Table A.3)

The CASSCF wavefunction of the **6S** isomer (Figure 3.4) with bent {Ge–C–Ge} fragment ( $C_{2v}$  symmetry) has a dominant contribution from the following CSF:

$$\Phi_1 = [\text{core}]12a_1^2 11b_1^2 13a_1^2 12b_2^2 14a_1^2 5b_1^2 13b_2^2 \quad |CI|^2 = 0.85$$

The next two dominant excitations,  $\Phi_2[14a_1^2 \rightarrow 15a_1^2]$  ( $|CI|^2 = 0.01$ ) and  $\Phi_3[5b_1^2 \rightarrow 6b_1^2]$  ( $|CI|^2 = 0.01$ ), correspond to transitions within  $\sigma$ - and  $\pi$ -orbital framework of the {Ge–C–Ge} fragment, respectively. The energy separation between **1S** and **6S** is 57.4 kcal mol<sup>-1</sup> (Table 3.3).

### 7S (Figure 3.4 and Table A.4)

The electronic state of the **7S** structure ( $C_s$  symmetry, in Figure 3.4) is mainly described by the configuration

$$\Phi_1 = [\text{core}]22a'^2 23a'^2 24a'^2 25a'^2 26a'^2 9a''^2 27a'^2 \quad |CI|^2 = 0.86$$

The next important double excitations are  $\Phi_2[9a''^2 \rightarrow 10a''^2]$  ( $|CI|^2 = 0.01$ ) and  $\Phi_3[27a'^2 \rightarrow 28a'^2]$  ( $|CI|^2 = 0.01$ ). The energy difference between the **7S** and **1S** isomers is 81.1 kcal mol<sup>-1</sup> Table 3.3, which is (23.7 kcal mol<sup>-1</sup>) higher than the preceding lower-lying structure **6S**.

### Transition States and Second-Order Saddle Points (Figure 3.5, Tables A.5-A.8)

The lowest-lying transition state structure **TS1** ( $C_{2v}$  symmetry, Figure 3.5) was predicted to be 18.7 kcal mol<sup>-1</sup> higher in energy than the global minimum **1S**. This transition state appears to connect two mirror images of isomer **3S** and has an equivalent electronic configuration.

The second transition state found on the PES is  $C_{2v}$  symmetric structure **TS2** (Figure 3.5). This isomer lies 87.9 kcal mol<sup>-1</sup> above the global minimum, with electron configuration similar to that of **6S**. **TS2** seems to connect two mirror images of isomer **7S**. Two stationary points of Hessian Index 2, **SSP1** and **SSP2**, were located on the PES. **SSP1** lies relatively low in energy at only 24.3kcal mol<sup>-1</sup> above the global minimum **1S**. The highest energy stationary point found in this study is **SSP2**, which has a relative energy of 102.3 kcal mol<sup>-1</sup> with respect to our global minimum.



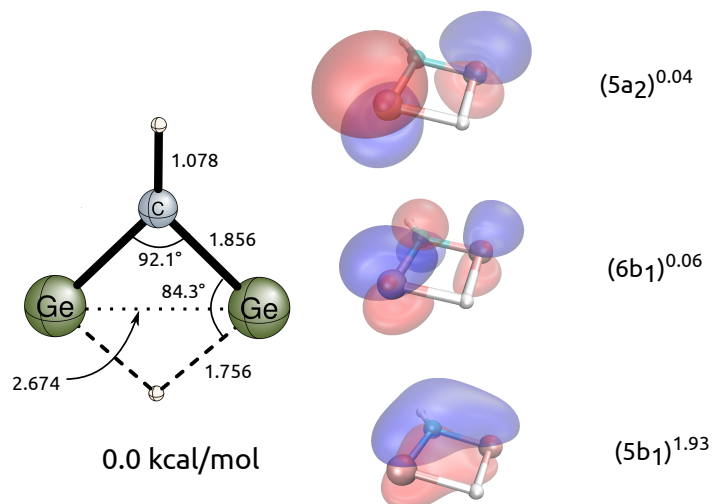


Figure 3.1: Geometry of the  $\text{Ge}_2\text{CH}_2$  global minimum structure **1S** ( $C_{2v}$  symmetry) optimized at the CCSD(T)/cc-pVQZ level of theory (on the left). Plots of its CASSCF frontier natural orbitals are shown on the right. The symmetries and the occupancies of three natural orbitals are also shown.

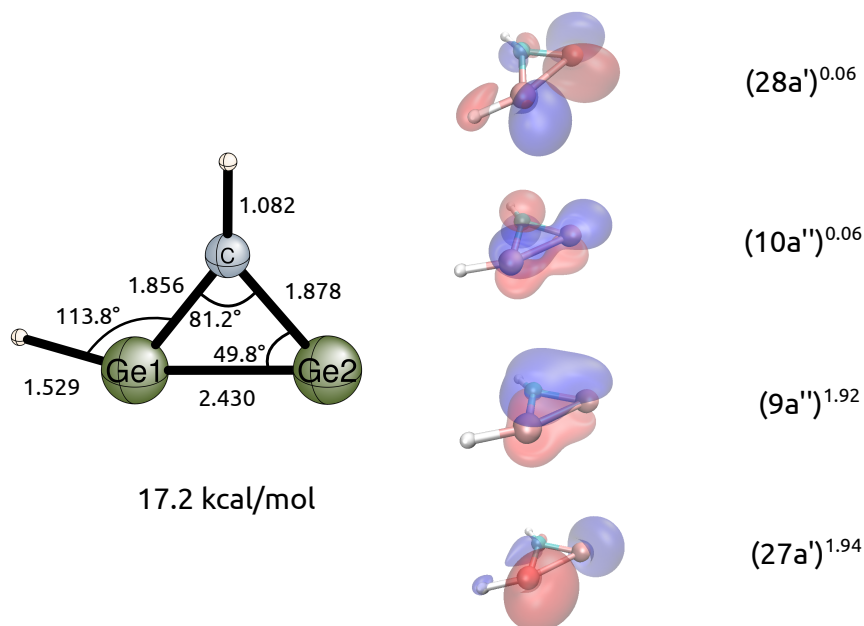


Figure 3.2: Geometry of the  $\text{Ge}_2\text{CH}_2$  isomer **2S** ( $C_s$  symmetry) optimized at the CCSD(T)/cc-pVQZ level of theory (on the left). Plots of its CASSCF frontier natural orbitals are shown on the right. The energy relative to the global minimum **1S** is computed at the CCSDT(Q)/CBS level of theory. The symmetries and the occupancies of four natural orbitals are also shown.

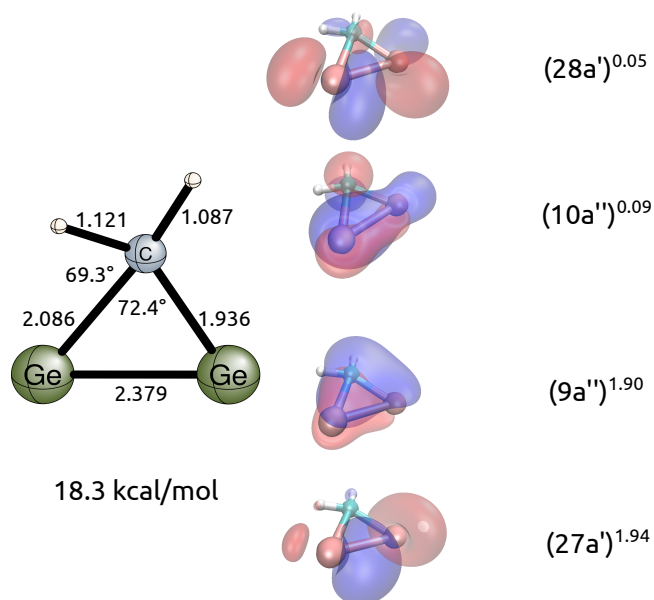


Figure 3.3: Geometry of the  $\text{Ge}_2\text{CH}_2$  isomer **3S** ( $C_s$  symmetry) optimized at the CCSD(T)/cc-pVQZ level of theory (on the left). Plots of the CASSCF frontier natural orbitals are shown on the right. The energy relative to the global minimum **1S** is computed at the CCSDT(Q)/CBS level of theory. The symmetries and the occupancies of four natural orbitals are also shown.

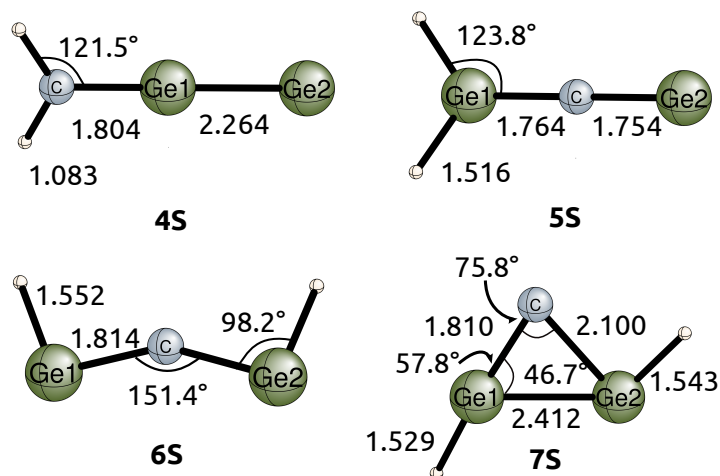


Figure 3.4: Geometries of the isomers **4S-7S** optimized at the CCSD(T)/cc-pVQZ level of theory.

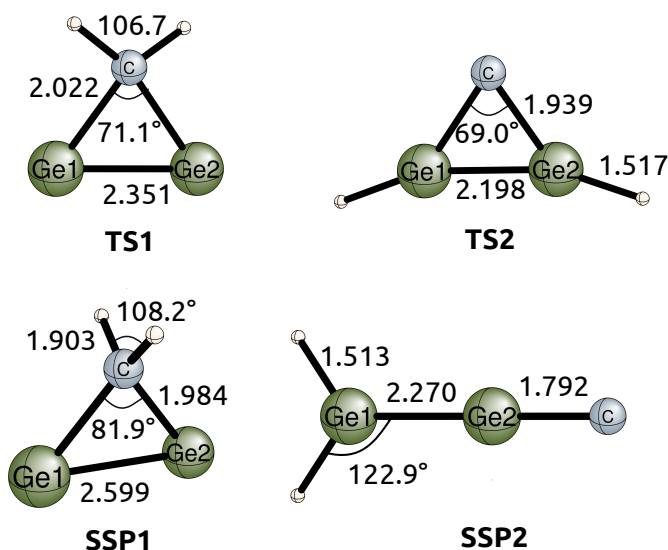


Figure 3.5: Geometries of the transition states **TS1-TS2**, and second-order saddle points **SSP1-SSP2** optimized at the CCSD(T)/cc-pVQZ level of theory.

Table 3.1: Focal Point Analysis of the Relative Energy Between Isomers **1S** and **2S** ( $\Delta E_{final}$ , kcal mol<sup>-1</sup>).<sup>a</sup>

	$\Delta E_e$ [RHF]	$+\delta$ MP2	$+\delta$ CCSD	$+\delta$ CCSD(T)	$+\delta$ CCSDT	$+\delta$ CCSDT(Q)	NET
cc-pVDZ	+18.05	+1.59	-0.29	+0.01	-0.06	-0.03	[+19.26]
cc-pVTZ	+18.22	+0.91	-0.38	+0.05	[-0.06]	[-0.03]	[+18.71]
cc-pVQZ	+18.25	+0.39	-0.41	+0.04	[-0.06]	[-0.03]	[+18.18]
cc-pV5Z	+18.27	+0.16	[-0.41]	[+0.04]	[-0.06]	[-0.03]	[+17.96]
CBS LIMIT	[+18.27]	[-0.09]	[-0.41]	[+0.04]	[-0.06]	[-0.03]	[+ <b>17.72</b> ]
$\Delta E_{final} = \Delta E_e[\text{CCSDT(Q)/CBS}] + \Delta_{\text{ZPVE}}[\text{CCSD(T)/cc-pVQZ}] + \Delta_{\text{CORE}}[\text{CCSD(T)/cc-pCVQZ}] + \Delta_{\text{DBOC}}[\text{CCSD/cc-pVTZ}] + \Delta_{\text{rel}}[\text{CCSD/cc-pVTZ}]$ $= +17.72 - 0.40 - 0.09 - 0.00 - 0.00 = \mathbf{17.23 \text{ kcal mol}^{-1}}$							

<sup>a</sup>The symbol  $\delta$  denotes the increment in the relative energy ( $\Delta E_e$ ) with respect to the preceding level of theory in the hierarchy SCF→MP2→CCSD→CCSD(T)→CCSDT→CCSDT(Q). Square brackets signify results obtained from basis set extrapolations or additivity assumptions. Final extrapolated values are boldfaced.

Table 3.2: Focal Point Analysis of the **3S** Isomer Relative Energy of Ge<sub>2</sub>CH<sub>2</sub> ( $\Delta E_{final}$ , kcal mol<sup>-1</sup>).<sup>a</sup>

	$\Delta E_e$ [RHF]	$+\delta$ MP2	$+\delta$ CCSD	$+\delta$ CCSD(T)	$+\delta$ CCSDT	$+\delta$ CCSDT(Q)	NET
cc-pVDZ	+21.98	-3.30	+0.77	-0.65	+0.07	-0.13	[+18.74]
cc-pVTZ	+21.73	-3.21	+1.14	-0.82	[+0.07]	[-0.13]	[+18.78]
cc-pVQZ	+21.92	-3.97	+1.47	-0.89	[+0.07]	[-0.13]	[+18.46]
cc-pV5Z	+21.89	-4.16	[+1.47]	[-0.89]	[+0.07]	[-0.13]	[+18.25]
CBS LIMIT	[+21.88]	[-4.36]	[+1.47]	[-0.89]	[+0.07]	[-0.13]	[+ <b>18.03</b> ]
$\Delta E_{final} = \Delta E_e[\text{CCSDT(Q)/CBS}] + \Delta_{\text{ZPVE}}[\text{CCSD(T)/cc-pVQZ}] + \Delta_{\text{core}}[\text{CCSD(T)/cc-pCVQZ}] + \Delta_{\text{DBOC}}[\text{CCSD(T)/cc-pVQZ}] + \Delta_{\text{rel}}[\text{CCSD(T)/cc-pVQZ}]$ $= +18.03 + 0.63 - 0.38 + 0.02 + 0.01 = \mathbf{18.31 \text{ kcal mol}^{-1}}$							

<sup>a</sup>The symbol  $\delta$  denotes the increment in the relative energy ( $\Delta E_e$ ) with respect to the preceding level of theory in the hierarchy SCF→MP2→CCSD→CCSD(T)→CCSDT→CCSDT(Q). Square brackets signify results obtained from basis set extrapolations or additivity assumptions. Final extrapolated values are boldfaced.

Table 3.3: The FPA extrapolated and final corrected energies (in kcal mol<sup>-1</sup>) for the eleven stationary points located on the singlet Ge<sub>2</sub>CH<sub>2</sub> potential energy surface

Structure	$\Delta E_{FPA}$	$\Delta E_{Final}$
<b>1S</b>	0.00	0.00
<b>2S</b>	17.72	17.23
<b>3S</b>	18.03	18.31
<b>4S</b>	30.88	31.69
<b>5S</b>	40.50	39.89
<b>6S</b>	61.02	58.05
<b>7S</b>	84.80	82.11
<b>TS1</b>	18.33	18.11
<b>TS2</b>	87.85	88.27
<b>SSP1</b>	24.34	22.57
<b>SSP2</b>	105.69	103.73

### 3.3.2 Geometries

The predicted geometries of isomers **1S-7S**, transition states **TS1-TS2**, and second-order saddle points **SSP1-SSP2** optimized at the CCSD(T)/cc-pVQZ level of theory are presented in Figure 3.1 to Figure 3.5.

#### Global Minimum **1S**

The global minimum structure on the  $\text{Ge}_2\text{CH}_2$  potential energy surface has an unusual cyclic arrangement containing one bridging hydrogen. In this isomer, the Ge–Ge bond distance decreases with advanced treatment of correlation effects to reach 2.674 Å at the highest level of theory as seen in Figure 3.1 and Figure S1. The reverse trend is observed with the C–Ge distance (1.856 Å) where the bond distance is stretched with increasing correlation level. On the other hand, the Ge–H distance in the bridged  $\text{Ge}\cdots\text{H}\cdots\text{Ge}$  bond shows a significant reduction of its length, as the correlation level increases owing it to its delocalized nature. The Ge–C–Ge angle in this isomer is  $92.1^\circ$  and the C–Ge–H angle has a magnitude of  $84.3^\circ$ . The Ge–Ge bond distance in the  $\text{Ge}_2\text{H}_2$  butterfly structure has been found to be 2.393 Å at the CCSD/DZP level of theory,<sup>51</sup> which is 0.28 Å shorter than in **1S**. This indicates a rather weak Ge–Ge interaction in the  $\text{Ge}_2\text{CH}_2$  global minimum. Consequently the Ge–H bond is also longer in the **1S** isomer.

#### **2S**

The **2S** isomer corresponds to the second lowest energy structure and is depicted in Figure 3.2 and Figure S2. It is another cyclic structure where the hydrogen atom forms only one bond to a germanium atom. The Ge–Ge bond distance shortens relative to **1S** by 0.2 Å to 2.430 Å at the CCSD(T)/cc-pVQZ level of theory. There is also a noticeable effect on the bond length upon more sophisticated treatments of correlation, since the Ge1–Ge2 bond length decreases by 0.29 Å when going from SCF/cc-pVQZ to CCSD(T)/cc-pVQZ level of theory.

A very significant dependence on the level of theory is observed on the Ge–C bond distances. At the SCF level of theory the Ge1–C and Ge2–C bond lengths are 1.917 Å and 1.801 Å, respectively. However when increasing the level of electron correlation treatment, the Ge1–C bond contracts to 1.856 Å and Ge2–C becomes the slightly longer bond with a distance of 1.878 Å. The Ge–C–Ge angle (81.2°) is noticeably smaller compared to the corresponding angle (92.1°) in **1S**. The analogous structure to **2S** in Ge<sub>2</sub>H<sub>2</sub> is the monobridged structure where one hydrogen is solely bonding to one germanium, while the other hydrogen is bridged between both germanium atoms. The Ge–Ge bond distance in this Ge<sub>2</sub>H<sub>2</sub> isomer is 2.268 Å (CCSD/DZP) which is again shorter than the 2.430 Å. However the Ge–H distance is comparable with 1.546 Å for the monobridged Ge<sub>2</sub>H<sub>2</sub> structure and 1.529 Å in **2S**.

### 3S

The **3S** cyclic structure is very close in energy to **2S** with the difference being only 1.08 kcal mol<sup>-1</sup>. In this structure the carbon atom has the two hydrogen atoms bound to it, as depicted in Figure 3.3 and Figure S3. The most remarkable features of **3S** are the tetravalent planar carbon and the unusually long C–H bond distance, 1.112 Å. The Ge1–Ge2 bond distance of 2.379 Å is 0.051 Å shorter than in **2S** at the CCSD(T)/cc-pVQZ level of theory. On the other hand, both of the Ge–C bond lengths (2.086 Å and 1.936 Å) are longer relative to **2S** (1.856 Å and 1.878 Å). Upon increasing level of correlation treatment the Ge1–C bond becomes slightly contracted, whereas the Ge2–C distance increases. The Ge–C–Ge bond angle is larger, in comparison to the same angle in **2S**, and amounts to 72.4°.

### 4S and 5S

The energetically lowest open chain isomer **4S** is shown in Figure 3.4 and Figure S4. In this gemrylidene structure the two hydrogen atoms form bonds with carbon. The two germanium lie on the same axis as carbon, resulting in a *C*<sub>2v</sub> symmetric structure. **4S** lies 32.0 kcal mol<sup>-1</sup>

higher in energy than the global minimum. The Ge-Ge bond distance of 2.264 Å is shorter than in all the aforementioned structures. The H-C-H bond angle is 116.9°. With higher level correlation treatments, the Ge-Ge bond distance decreases, while the Ge-C increases. Structure **5S** in Figure 3.4 and Figure S5 also has a non-cyclic structure. In this isomer the two hydrogen atoms are bound to germanium and the carbon atom is the central part of the Ge-C-Ge backbone. The Ge-C bond lengths are 1.764 Å and 1.754 Å. The effects of higher correlation treatments are analogous to those in **4S**.

### **6S and 7S (in Figure 3.4, S6 and S7)**

The two highest lying minima (equilibrium) structures are the carbene-like isomers **6S** and **7S**. In **6S** (Figure 3.4 and Figure S6) the Ge-C bond distance is 1.814 Å which is comparable to the Ge-C bond length in structures **4S** and **5S**. The most noteworthy parameter in **6S** is the wide Ge-C-Ge angle. A considerable variation is observed with increasing level of correlation treatment. The angle decreases from 172° at the SCF/cc-pVQZ level of theory to 151° at CCSD(T)/cc-pVQZ. Finally, the cyclic **7S** isomer (Figure 3.4 and Figure S7) is the highest lying minimum on the singlet PES. The Ge-Ge bond distance of 2.412 Å is comparable to that in the other cyclic structures **2S** and **3S**. This bond length decreases with advanced treatment of correlation. The C-Ge1 bond (1.810 Å) is noticeably shorter than the C-Ge2 (2.100 Å), which is the largest difference between lengths of the two Ge-C bond distances among the cyclic isomers.

### **TS1 and TS2**

Structure **TS1** (Figure 3.5 and Figure S8) is a  $C_{2v}$  symmetry transition state with one imaginary vibrational frequency corresponding to the CH<sub>2</sub> rocking motion. This normal mode connects the two mirror images of the **3S** isomer. For this reason the structural features of **TS1** and dependence on correlation treatment of geometrical parameters resemble those

of **3S**. The second transition state found on this PES is the  $C_{2v}$  **TS2** structure (Figure 3.5 and Figure S9). This transition state connects two identical **7S** isomers, through a *trans*-HGeGeH bending motion. A noteworthy difference between **TS2** and **7S** is the different lengths of the Ge–Ge bond. The Ge–Ge bond distance of 2.198 Å in **TS2** is the shortest Ge–Ge bond among all stationary points located in this study. This is consistent Ge=Ge double bond that one would associate with the valance isoelectronic cyclopropenylidene.

### SSP1 and SSP2

Lastly, two stationary points of Hessian index 2 were found on the singlet PES. The lower in energy is the cyclic **SSP1** (Figure 3.5 and Figure S10) and it is the only non-planar stationary point. The Ge–Ge bond (2.599 Å) is quite elongated, second only to the global minimum **1S**, thus suggesting a rather weak Ge–Ge single bond. This bond distance decreases with increasing level of correlation, following the trend observed for the other cyclic isomers. The **SSP2** structure (Figure 3.5 and Figure S11) is the highest lying stationary point found in this study. It is a non-cyclic vinylidene structure with a terminal carbon and both germanium atoms on the  $C_2$  symmetry axis.

### 3.3.3 Harmonic Vibrational Frequencies

The nature of the stationary points has been characterized through harmonic vibrational frequency analysis. Seven minima, two transition states, and two second order saddle points were identified among the 11 stationary points considered in this study. The harmonic vibrational frequencies (in wavenumbers) of the nine normal modes together with ZPVE at the CCSD(T) cc-pVQZ level of theory are given in Table 3.4. The stationary points **1S** through **7S** were found to have all real frequencies at every levels of theory. The only exception is **7S** which is a transition state at the SCF level of theory and once correlation effects are added it becomes a minimum on the PES. The imaginary frequency of **TS1**



corresponds to a rocking motion of the  $\text{CH}_2$  group. This transition state connects the mirror images of **3S** structure. The imaginary frequency of **TS2** is associated with a trans  $\text{HGeGeH}$  bending motion. This transition state connects the two mirror images of the **7S** carbene isomer. Finally, the two imaginary frequencies detected for the second order saddle point **SSP1** correspond to an out of plane rocking motion and a twisting motion of the  $\text{CH}_2$  group. For **SSP2** the two imaginary frequencies may be assigned to an out-of plane and an in-plane bending  $\text{Ge-Ge-C}$  motions.

Table 3.4: Harmonic vibrational frequencies (in  $\text{cm}^{-1}$ ) and the ZPVE (in  $\text{kcal mol}^{-1}$ ) for the 11  $\text{Ge}_2\text{CH}_2$  structures at the CCSD(T) cc-pVQZ level of theory

Structures	Energy	Symmetry	$\omega_1$	$\omega_2$	$\omega_3$	$\omega_4$	$\omega_5$	$\omega_6$	$\omega_7$	$\omega_8$	$\omega_9$	ZPVE
<b>1S</b>	-4190.507579	$C_{2v}$	3250( $a_1$ )	1435( $a_1$ )	763( $a_1$ )	268( $a_1$ )	852( $b_1$ )	463( $b_1$ )	1100( $b_2$ )	755( $b_2$ )	668( $b_2$ )	13.66
<b>2S</b>	-4190.478460	$C_s$	3202( $a'$ )	2121( $a'$ )	837( $a'$ )	778( $a'$ )	669( $a'$ )	374( $a'$ )	194( $a'$ )	748( $a''$ )	353( $a''$ )	13.26
<b>3S</b>	-4190.478052	$C_s$	3147( $a'$ )	2763( $a'$ )	1428( $a'$ )	647( $a'$ )	414( $a'$ )	385( $a'$ )	236( $a'$ )	714( $a''$ )	259( $a''$ )	14.29
<b>4S</b>	-4190.453764	$C_{2v}$	3135( $a_1$ )	1382( $a_1$ )	763( $a_1$ )	302( $a_1$ )	711( $b_1$ )	39( $b_1$ )	3242( $b_2$ )	713( $b_2$ )	60( $b_2$ )	14.79
<b>5S</b>	-4190.445568	$C_{2v}$	2227( $a_1$ )	1269( $a_1$ )	893( $a_1$ )	339( $a_1$ )	525( $b_1$ )	86( $b_1$ )	2223( $b_2$ )	582( $b_2$ )	128( $b_2$ )	11.83
<b>6S</b>	-4190.408783	$C_{2v}$	2044( $a_1$ )	630( $a_1$ )	374( $a_1$ )	116( $a_1$ )	527( $a_2$ )	124( $b_1$ )	2034( $b_2$ )	960( $b_2$ )	196( $b_2$ )	10.02
<b>7S</b>	-4190.369076	$C_s$	2087( $a'$ )	2047( $a'$ )	784( $a'$ )	644( $a'$ )	423( $a'$ )	281( $a'$ )	178( $a'$ )	341( $a''$ )	156( $a''$ )	9.92
<b>TS1</b>	-4190.477410	$C_{2v}$	3074( $a_1$ )	1323( $a_1$ )	585( $a_1$ )	305( $a_1$ )	256( $a_2$ )	711( $b_1$ )	3122( $b_2$ )	415( $b_2$ )	213i( $b_2$ )	14.0
<b>TS2</b>	-4190.364368	$C_{2v}$	2170( $a_1$ )	737( $a_1$ )	517( $a_1$ )	354( $a_1$ )	337( $a_2$ )	342( $b_1$ )	2174( $b_2$ )	524( $b_2$ )	127i( $b_2$ )	10.23
<b>SSP1</b>	-4190.467149	$C_{2v}$	3042( $a_1$ )	1282( $a_1$ )	617( $a_1$ )	223( $a_1$ )	304i( $a_2$ )	3103( $b_1$ )	449i( $b_1$ )	803( $b_2$ )	460( $b_2$ )	13.62
<b>SSP2</b>	-4190.332438	$C_{2v}$	2225( $a_1$ )	847( $a_1$ )	831( $a_1$ )	288( $a_1$ )	300( $b_1$ )	62i( $b_1$ )	2247( $b_2$ )	427( $b_2$ )	27i( $b_2$ )	10.24

## 3.4 Natural Bond Orbital Analyses

### 3.4.1 Isomer 1S

In order to get better insights, concerning the bonding nature of the different isomers NBO analyses were performed. All isomers have 14 valence electrons participating in bonding. At first sight, two very peculiar features can be noticed in the structure of the intriguing **1S** isomer: 1) The hydrogen atom bridging the two germanium atoms and 2) an unusually elongated Ge–Ge bond length of 2.674 Å at our highest level of theory.

Figure 3.6 depicts the several structures predicted by NBO. With respect to the first point above, NBO renders a three-center two-electron Ge–H–Ge  $\sigma$  bond, with an occupation number of 1.97. There is very little hybridization on the germanium atoms since the orbitals participating in the three-center two-electron bond have 95% p-character (Table A.9). This is in good agreement with the C–Ge–H bond angle of 84.3 ° which is close to the angle of 90° in pure atomic p-orbitals. The Ge–C  $\sigma$ -bonds are primarily composed of p-orbitals (86% p-character) on the germanium atoms and  $sp^{2.15}$  hybrids on the carbon atom. Furthermore, both germanium atoms have a lone pair 4s orbital, which mixes little with the p-orbitals (84% s-character). Another noteworthy feature of **1S** is a three-center two-electron  $\pi$  bond spanning over the Ge–C–Ge ring. NBO predicts that the orbitals involved in this bond are the out-of-plane p-orbital on carbon and on the two germaniums. The carbon p-orbital provides one electron, and one p-orbital on germanium contributes with another electron, thus forming a three-center two-electron  $\pi$ -bond with a total occupation of 1.99. Inasmuch as there are two electrons delocalized over a three membered ring and according to Hückels  $4n+2$  electron rule, this bond should be  $\pi$  aromatic.

The unusually elongated Ge–Ge bond can be rationalized by analyzing the bonds predicted by NBO. There is no evidence for a  $\sigma$  bond between the adjacent germanium atoms. The eight valence electrons of the two germanium atoms are incorporated into the two Ge–C

bonds (2 electrons), the two lone pairs (4 electrons), one three-center two-electron Ge–H–Ge  $\sigma$ -bond (1 electron), and one three-center two-electron Ge–C–Ge  $\pi$  bond (1 electron). Moreover, the Ge–Ge Wiberg bond order of 0.46, can mainly be ascribed to the three-center two-electron  $\pi$  aromatic bond.

In summary, the in-plane hydrogen bridged Ge–H–Ge bond allows the germanium atoms to form bonds without the need of hybridization, since the C–Ge–H bond angle is  $84.3^\circ$  very close to the  $90^\circ$  angle of atomic p-orbitals, thus forming strong  $\sigma$  bonds<sup>48</sup>. Additionally, the out-of-plane  $\pi$  bond, due to its  $\pi$  aromatic nature, contributes further in stabilizing the **1S** isomer. The synchronicity of energetically favorable effects make this remarkable isomer the global minimum on the Ge<sub>2</sub>CH<sub>2</sub> PES.

### 3.4.2 Isomer 2S

The second lowest lying isomer **2S** has the same cyclic backbone as **1S**, but one hydrogen atom is now bonding solely to one germanium, while the other is bonded to the carbon atom. Figure 3.6 shows the structure obtained by the NBO analysis. As for **1S**, NBO predicts for **2S** an out-of-plane three-center two-electron Ge–C–Ge aromatic  $\pi$  bond (Table A.10). The other similarities are the Ge–C  $\sigma$  bonds, which are formed by mainly unmixed p-orbitals (86% p-character) on the germanium side and sp<sup>2</sup>-hybrids on carbon (Table A.10). The biggest difference with respect to **1S** is the absence of the three-center two-electron  $\sigma$ -bond, which results in the necessity of s and p orbital mixing on one germanium in order to form two sp-hybrids (Figure 3.6 middle panel). One of these sp-hybrids is used to form the Ge–H  $\sigma$ -bond, while the right hand germanium is part of a Ge–Ge  $\sigma$ -bond. On the other germanium, little s- and p-orbital mixing is observed, and the Ge–Ge and Ge–C  $\sigma$ -bonds are formed mainly with p-orbitals whereas the s-orbital holds a lone pair.

### 3.4.3 Isomer 3S

In structure **3S** both hydrogen atoms are bound to the carbon atom, which results in a planar tetracoordinated carbon (ptC) atom. Compounds possessing planar tetravalent carbon have been subject of a myriad of studies<sup>140–143</sup> The most favorable configuration for this type of compounds has been found to be a  $sp^2$ -hybridized central carbon which forms electron deficient  $\sigma$ -bonds, having 6 electrons available for four bonds, while the remaining two electrons occupy in the out-of-plane p-orbital. The reason for the preferred planar structure in **3S** appears to be the incorporation of the ptC into the three membered ring. This allows the out-of-plane lone pair on the carbon to delocalized into the empty out-of-plane p-orbitals on the two germaniums in order to form a  $\pi$  aromatic three membered ring as in **1S** and **3S** ( Figure 3.6 lower panel). Moreover the 6 electron  $\sigma$  framework involving the carbon is composed of two C-H  $\sigma$ -bonds with 2 electrons, respectively and a second three-center two-electron bond composed of radially overlapping p-orbitals on the germaniums (90% p-character) and an sp-hybrid on the carbon atom (Table A.11 and Figure 3.6 middle panel). Thus the carbon atom acts as a  $\pi$  electron donor and  $\sigma$  electron acceptor within the ring.

### 3.4.4 Isomer 4S and 5S

The lowest lying non-cyclic structure corresponds to the **4S** isomer. NBO analysis gives as expected a near  $sp^2$  hybridization on the carbon atom (Table S12). Furthermore, NBO renders a Ge-C and Ge-Ge  $\pi$ -bond and a lone pair on the terminal Ge atom. The bonding pattern of **5S** is similar to **4S** in the sense that two  $\pi$ -bonds and a lone pair are present, the difference being that they are both Ge-C bonds (Table S13). Structure **4S** lies 6.67 kcal/mol lower than **5S** at our highest level of theory. A possible explanation of this energy ordering could be hybridization, since in **4S** the atom bonding to the two hydrogens is a carbon atom, where  $sp^2$  hybridization is preferred. On the other hand in **5S** a germanium atom

has to undergo the, due to size differences between carbon and germanium, energetically unfavorable process of p and s orbital mixing in order to bond to the two hydrogen atoms.

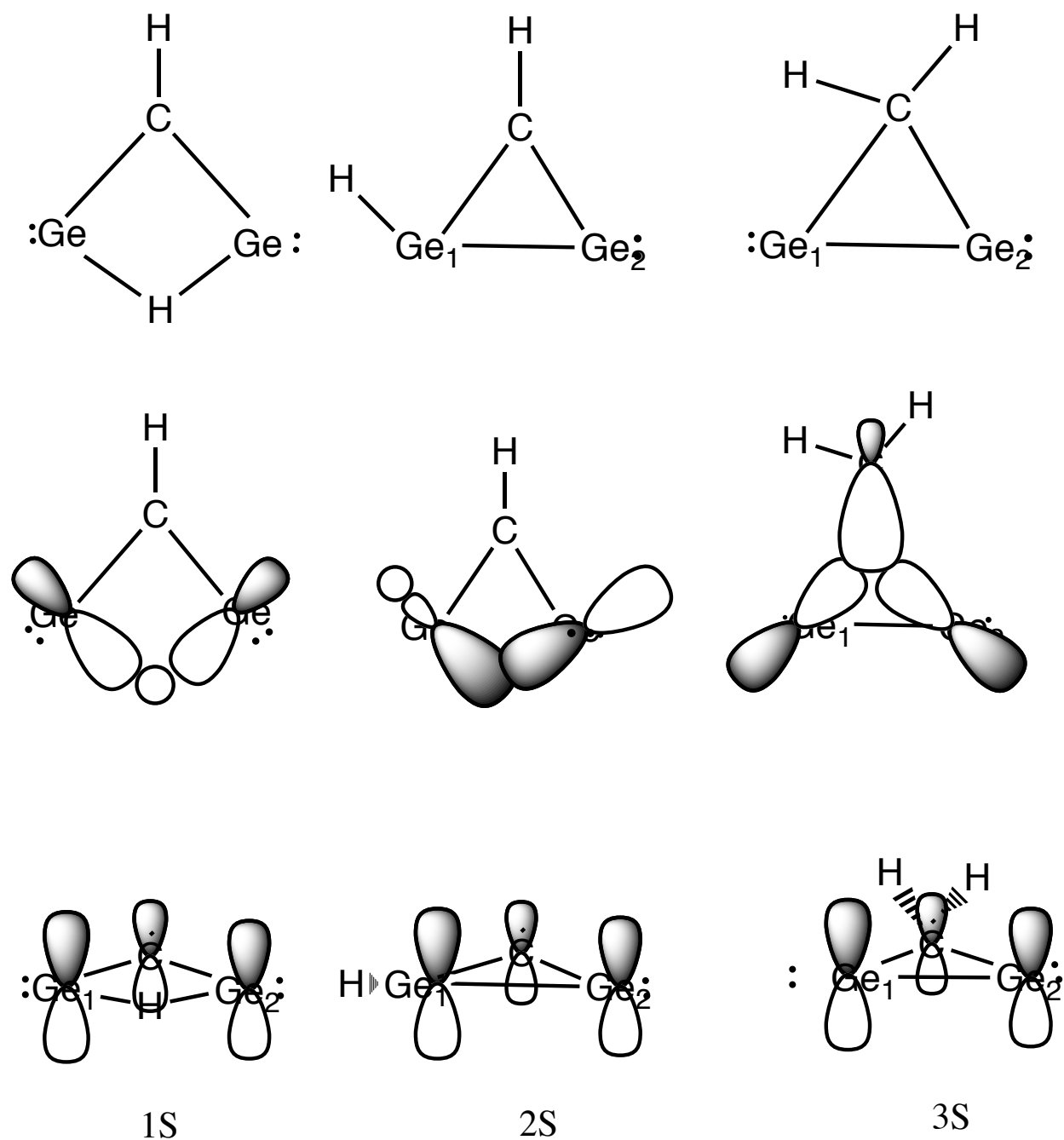


Figure 3.6: Depiction of the bonding structures predicted by the NBO analyses. Upper panel: Lewis type structures for the three lowest lying isomer **1S**, **2S**, and **3S**. Middle panel: The Ge-H-Ge three-center two-electron bond on **1S**, the Ge<sub>1</sub>-Ge<sub>2</sub>  $\sigma$ -bond, the Ge<sub>1</sub>-H bond on **2S** and the radial in plane three-center two-electron Ge-C-Ge bond on **3S**. Lower panel: The out-of-plane three-center two-electron  $\pi$ -bonds for **1S**, **2S**, and **3S**.

## 3.5 Aromaticity

The three lowest lying isomers (**1S**–**3S**) incorporate a three membered ring together with two  $\pi$ -electrons. Consequently, they can be regarded as Hückel aromatic. In order to dwell deeper into the aromatic nature of the three cyclic structures, the NICS(0) $_{\pi zz}$  and NICS(0) value were computed (Figure 3.7). According to this aromaticity criterion, all three isomers are found to be aromatic, since negative NICS(0) values can be associated with aromaticity. The NICS(0) $_{\pi zz}$  value, which is the best indicator for  $\pi$  aromaticity is noticeably higher in **1S** (18.72 ppm) than in **2S** or **3S** (8.91 ppm and 8.04 ppm respectively), making it the most  $\pi$  aromatic isomer. Moreover, the NICS(0) $_{\pi zz}$  values correlate well with the relative energy difference indicating that aromatic stabilization energy could be a preponderant factor in the energy ordering of the cyclic isomers. Although the NICS(0) $_{\pi zz}$  of **2S** and **3S** is similar, the NICS(0) values are separated by almost 10 ppm. This difference could be attributed to the in plane three-center two-electron bond predicted by the NBO analysis. This delocalized radial bond is only present in **3S** and would contribute to the NICS(0), while not contained in the NICS(0) $_{\pi zz}$  value.



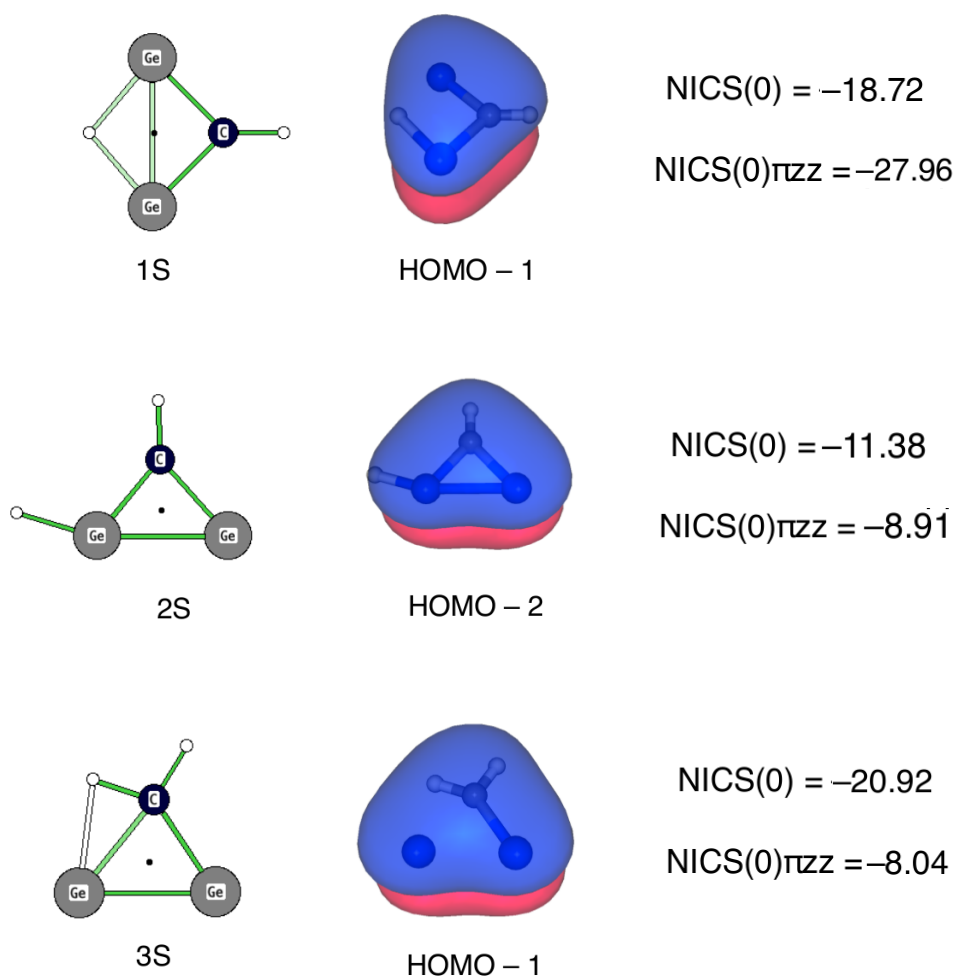


Figure 3.7:  $\text{NICS}(0)$  and  $\text{NICS}(0)_{\pi_{zz}}$  values in ppm for the isomers **1S**, **2S** and **3S** taken at the center of the rings. A negative  $\text{NICS}(0)$  value indicates diatropic shielding and aromaticity. The orbitals used to compute the dissected  $\text{NICS}(0)_{\pi_{zz}}$  are also shown.

## 3.6 Concluding Remarks

Through the use of state-of-the-art *ab initio* electronic structure theory, the lowest singlet potential energy structure of  $\text{Ge}_2\text{CH}_2$  was systematically investigated. Eleven stationary points are found among which there are seven minima, two transition states, and two second order saddle points. After focal point analysis and adding ZPVE, DBOC, core and relativistic corrections, the energy ordering of the seven minima is predicted to be: **1S** [0.0]<**2S** [17.23]<**3S** [18.31]<**4S** [31.69]<**5S** [39.89]<**6S** [58.05]<**7S** [82.11]. The findings about the electronic structure of the seven minima indicates the following:

1. Cyclic arrangements as in **1S**, **2S** and **3S** are the energetically most favourable structures for the  $\text{Ge}_2\text{CH}_2$  system
2. There is little mixing of s and p orbitals on germanium, and formation of three-center two-electron bonds, is energetically preferred.
3. The absence of a Ge-Ge bond and two out-of-plane three-center two-electron bonds make **1S** a remarkable structure.
4. An isomer incorporating a rare planar tetracoordinated carbon is found among the low energy minima
5. The carbene-like structures are the least favored on the  $\text{Ge}_2\text{CH}_2$  PES.
6. The three lowest lying cyclic (**1S**–**3S**) structures are found to be aromatic

We hope that our predictions will encourage future experimental investigations on these novel digermanium compounds.

## 3.7 Acknowledgments

This research was supported by the U.S. National Science Foundation Grant CHE-1054286.

# Chapter 4

## Summary and Conclusions

The use of a variety of *ab initio* methods paired with wavefunction and energy analysis tools has provided deep insight into the electronic structure and chemistry of molecules containing phosphorous and germanium. In the first part of our research, we endeavoured into the chemistry of phosphorous, with the particular goal of finding a substituent that is capable of reversing the diphosphene-diphosphylydene energetic order. After probing 29 different substituents of varying nature, it was found that lithoxy substituted diphosphylydene lies 33 kcal/mol lower than the equivalent diphosphene isomer. Furthermore isodesmic reaction energies were obtained for the mono- and di-substitution in order to isolate the energetic effect associated with the substitution of hydrogen by a functional group. By comparing the energies of both reaction schemes, it was seen that with the replacement of both hydrogens the energy gap could be reduced while by substituting only one hydrogen, the energy gap was mainly unaffected. It was found that the drastic effect of the second substituents can be attributed to an enhanced coulombic interaction in the diphosphylydene type structures. This favourable charge distribution is not present in the diphosphene isomer and hence the diphosphylydene becomes the energetically preferred structure.

Our second incursion into the world of main group chemistry was studying the potential

energy surface of  $\text{Ge}_2\text{CH}_2$ . A stochastic procedure named “kick“ was employed in order to systematically explore the potential energy surface in the quest for exotic structures. Eleven stationary points were found of which seven correspond to minima. CCSD(T)/cc-pVQZ geometries were computed for all stationary points and focal point energies were obtained. The three lowest lying isomers have a three membered ring, and the final energies were found to be: **1S** = 0.0 kcal mol<sup>-1</sup>, **2S** = 17.23 kcal mol<sup>-1</sup> **3S** = 18.31 kcal mol<sup>-1</sup>. A rare planar tetracoordinated carbon was found in the **3S** isomer. Using NBO analysis we found that three-center two-electron bonds are ubiquitous in the low energy structures, regardless whether they are of  $\sigma$  or  $\pi$  nature. Finally, NICS analysis predicted aromaticity for all three low lying cyclic structures, where the amount of the chemical shift correlated well with the energy difference, thus hinting at a important role of aromatic stabilization in the energy ordering.

# Bibliography

- [1] Schrödinger, E. *Ann. Phys.* **1926**, *386*, 109–139.
- [2] Born, M.; Oppenheimer, R. *Ann. Phys.* **1927**, *389*, 457–484.
- [3] Slater, J. C. *Quantum theory of atomic structure*; McGraw-Hill New York, 1960; Vol. 2.
- [4] Pauli, W. *Z. Phys* **1925**, *31*, 765–783.
- [5] Fock, V. *Z. Physik* **1930**, *61*, 126–148.
- [6] Hartree, D. R.; Hartree, W.; Swirles, B. *Phil. Trans.* **1939**, *238*, 229–247.
- [7] Hartree, D.; Hartree, W. *Proc. R. Soc. A* **1948**, *193*, 299–304.
- [8] Roothaan, C. C. J. *Rev. Mod. Phys.* **1951**, *23*, 69–89.
- [9] Hall, G. G. *Proc. R. Soc. A* **1951**, *205*, pp. 541–552.
- [10] Szabo, A.; Ostlund, N. S. *Modern Quantum Chemistry: Introduction to Advanced Electronic Structure Theory (Dover Books on Chemistry)*, new edition ed.; Dover Publications, 1996.
- [11] Čížek, J.; Paldus, J.; Šroubková, L. *Int. J. Quant. Chem.* **1969**, *3*, 149–167.
- [12] Crawford, T. D.; Schaefer, H. F. *An Introduction to Coupled Cluster Theory for Computational Chemists*; John Wiley & Sons, Inc., 2007; pp 33–136.

- [13] Bartlett, R. J.; Purvis, G. D. *Int. J. Quant. Chem.* **1978**, *14*, 561–581.
- [14] Rittby, M.; Bartlett, R. J. *J. Phys. Chem.* **1988**, *92*, 3033–3036.
- [15] Purvis, G. D.; Bartlett, R. J. *J. Chem. Phys.* **1982**, *76*, 1910–1918.
- [16] Raghavachari, K.; Trucks, G. W.; Pople, J. A.; Head-Gordon, M. *Chem. Phys. Lett.* **1989**, *157*, 479–483.
- [17] Stanton, J. F. *Chem. Phys. Lett.* **1997**, *281*, 130–134.
- [18] Watts, J. D.; Gauss, J.; Bartlett, R. J. *Chem. Phys. Lett.* **1992**, *200*, 1–2.
- [19] Watts, J.; Gauss, J.; Bartlett, R. J. *J. Chem. Phys.* **1993**, *98*, 8718–8733.
- [20] Császár, A. G.; Allen, W. D.; Schaefer, H. F. *J. Chem. Phys.* **1998**, *108*, 9751–9764.
- [21] Schuurman, M. S.; Muir, S. R.; Allen, W. D.; Schaefer, H. F. *J. Chem. Phys.* **2004**, *120*, 11586–11599.
- [22] Gonzales, J. M.; Pak, C.; Cox, R. S.; Allen, W. D.; Schaefer, H. F.; Császár, A. G.; Tarczay, G. *Chem. Eur. J.* **2003**, *9*, 2173–2192.
- [23] Császár, A. G.; Tarczay, G.; Leininger, M. L.; Polyansky, O. L.; Tennyson, J.; Allen, W. D. In *Spectroscopy from Space*; Demaison, J.; Sarka, K., Eds.; Kluwer: Dordrecht, 2001; p 317.
- [24] Dunning, T. H. *J. Chem. Phys.* **1989**, *90*, 1007–1023.
- [25] Wilson, A. K.; van Mourik, T.; Dunning, T. H. *J. Mol. Struct.* **1996**, *388*, 339–349.
- [26] Kato, T. *Comm. Pure Appl. Math.* **1957**, *10*, 151–177.
- [27] Perera, S. A.; Bartlett, R. J. *Chem. Phys. Lett.* **1993**, *216*, 606–612.

- [28] Handy, N. C.; Yamaguchi, Y.; Schaefer, H. F. *J. Chem. Phys.* **1986**, *84*, 4481–4484.
- [29] Parr, R.; Yang, W. *Density Functional Theory of Atoms and Molecules*; Oxford University Press: New York., 1989.
- [30] Thomas, L. H. *Math. Proc. Cambridge Philos. Soc.* **1927**, *23*, 542–548.
- [31] Fermi, E. *Rend. Accad. Naz. Lincei* **1927**, *6*, 602–607.
- [32] Hohenberg, P.; Kohn, W. *Phys. Rev. B* **1964**, *136*, 864–871.
- [33] Kohn, W.; Sham, L. *Phys. Rev.* **1965**, *140*, 1133.
- [34] Becke, A. *J. Chem. Phys.* **1993**, *98*, 5648–5652.
- [35] Lee, C.; Yang, W.; Parr, R. *Phys. Rev. B* **1988**, *37*, 785.
- [36] Becke, A. D. *Phys. Rev. A* **1988**, *38*, 3098–3100.
- [37] Perdew, J. P.; Burke, K.; Ernzerhof, M. *Phys. Rev. Lett.* **1997**, *78*, 1396–1396.
- [38] Tao, J.; Perdew, J. P.; Staroverov, V. N.; Scuseria, G. E. *Phys. Rev. Lett.* **2003**, *91*, 146401.
- [39] Handy, N. C.; Cohen, A. J. *Mol. Phys.* **2001**, *99*, 403–412.
- [40] Zhao, Y.; Schultz, N. E.; Truhlar, D. G. *J. Chem. Phys.* **2005**, *123*, 161103.
- [41] Zhao, Y.; Schultz, N. E.; Truhlar, D. G. *J. Chem. Theory Comput.* **2006**, *2*, 364–382.
- [42] Foster, J. P.; Weinhold, F. *J. Am. Chem. Soc.* **1980**, *102*, 7211–7218.
- [43] Reed, A. E.; Curtiss, L. A.; Weinhold, F. *Chem. Rev.* **1988**, *88*, 899–926.
- [44] WEINHOLD, F.; Landis, C. R. *Chem. Educ. Res. Pract.* **2001**, *2*, 91–104.

- [45] Weinhold, F.; Landis, C. R. *Valency and bonding: a natural bond orbital donor-acceptor perspective*; Cambridge University Press, 2005.
- [46] Lewis, G. N. *J. Am. Chem. Soc.* **1916**, *38*, 762–785.
- [47] Reed, A. E.; Weinstock, R. B.; Weinhold, F. *J. Chem. Phys.* **1985**, *83*, 735–746.
- [48] Kutzelnigg, W. *Angew. Chem. Int. Ed.* **1984**, *23*, 272–295.
- [49] Wells, A. F.; *Structural Inorganic Chemistry*; 1986.
- [50] Colegrove, B. T.; Schaefer, H. F. I. *J. Phys. Chem.* **1990**, *94*, 5593–5602.
- [51] Palagyi, Z.; Schaefer, H. F.; Kapuy, E. *J. Am. Chem. Soc.* **1993**, *115*, 6901–6903.
- [52] Davidson, P. J.; Lappert, M. F. *J. Chem. Soc. Chem. Commun.* **1973**, 317.
- [53] Goldberg, D. E.; Harris, D. H.; Lappert, M. F.; Thomas, K. M. *J. Chem. Soc. Chem. Commun.* **1976**, 261–262.
- [54] West, R.; Fink, M. J.; Michl, J. *Science* **1981**, *214*, 1343–1344.
- [55] Sekiguchi, A.; Kingo, R.; Ichinohe, M. *Science* **2004**, *305*, 1755–1757.
- [56] Stender, M.; Phillips, A. D.; Wright, R. J.; Power, P. P. *Angew. Chem. Int. Ed.* **2002**, *41*, 1785–1787.
- [57] Seyferth, D. *Organometallics* **2001**, *20*, 2–6.
- [58] Spies, P. *Angew. Chem. Int. Edn* **2008**, *47*, 7543–7546.
- [59] Power, P. P. *Nature* **2010**, *463*, 171–177.
- [60] Coyle, E. E.; O’Brien, C. J. *Nature Chemistry* **2012**, *4*, 779–780.
- [61] Nitschke, J. R. *Nature Chemistry* **2011**, *3*, 90.



- [62] Fritz, G.; Scheer, P. *Chem. Rev.* **2000**, *100*, 3341–3402.
- [63] Olkowska-Oetzel, J.; Pikies, J. *App. Organomet. Chem.* **2003**, *17*, 28–35.
- [64] Pikies, J.; Baum, E.; Matern, E.; Chojnacki, J.; Grubba, R.; Robaszkiewicz, A. *Chem. Comm.* **2004**, 2478–2479.
- [65] Matus, M. H.; Nguyen, M. T.; Dixon, D. A. *J. Phys. Chem. A* **2007**, *111*, 1726–1736.
- [66] Norman, N. *Polyhedron* **1993**, *12*, 2431–2446.
- [67] Back, O.; Donnadieu, B.; Parameswaran, P.; Frenking, G.; Bertrand, G. *Nature Chemistry* **2010**, *2*, 369–373.
- [68] Yoshifuji, M.; Shima, I.; Inamoto, N.; Hirotsu, K. *J. Am. Chem. Soc.* **1981**, *103*, 4587–4589.
- [69] Escudie, J.; Couret, C.; Andriamizaka, J. D.; Satge, J. *J. Organomet. Chem.* **1982**, *228*, C76–C78.
- [70] Niecke, E.; Rüger, R.; Lysek, M.; Pohl, S.; Schoeller, W. *Angew. Chem. Int. Ed.* **1983**, *22*, 486–487.
- [71] Sasamori, T.; Takeda, N.; Tokitoh, N. *J. Phys. Org. Chem.* **2003**, *16*, 450–462.
- [72] Yoshifuji, M.; Shibayama, K.; Inamoto, N.; Matsushita, T.; Nishimoto, K. *J. Am. Chem. Soc.* **1983**, *105*, 2495–2497.
- [73] Wang, Y.; Xie, Y.; Wei, P.; King, R. B.; Schaefer, H. F.; Schleyer, P. v. R.; Robinson, G. H. *J. Am. Chem. Soc.* **2008**, *130*, 14970–14971.
- [74] Hamaguchi, H.; Tasumi, M.; Yoshifuji, M.; Inamoto, N. *J. Am. Chem. Soc.* **1984**, *106*, 508–509.

- [75] Partyka, D. V.; Washington, M. P.; Gray, T. G.; Updegraff, J. B.; Turner, J. F.; Protasiewicz, J. D. *J. Am. Chem. Soc.* **2009**, *131*, 10041–10048.
- [76] Nguyen, M. T. *Chem. Phys. Lett.* **1987**, *135*, 73–77.
- [77] Nguyen, M. T.; Van Keer, A.; Vanquickenborne, L. G. *J. Org. Chem.* **1996**, *61*, 7077–7084.
- [78] Schmidt, M. W.; Gordon, M. S. *Inorg. Chem.* **1986**, *25*, 248–254.
- [79] Jin, S.; Colegrove, B. T.; Schaefer, H. F. *Inorg. Chem.* **1991**, *30*, 2969–2977.
- [80] Busch, T.; Schoeller, W. W.; Niecke, E.; Nieger, M.; Westermann, H. *Inorg. Chem.* **1989**, *28*, 4334–4340.
- [81] Allen, T. L.; Scheiner, A. C.; Yamaguchi, Y.; Schaefer, H. F. *Chem. Phys. Lett.* **1985**, *121*, 154–158.
- [82] Nguyen, M. T. *Chem. Phys. Lett.* **1986**, *109*, 277–288.
- [83] Lu, T.; Simmonett, A. C.; Evangelista, F. A.; Yamaguchi, Y.; Schaefer, H. F. *J. Phys. Chem. A* **2009**, *113*, 13227–13236.
- [84] Shao, Y.; et al. *Phys. Chem. Chem. Phys.* **2006**, *8*, 3172–3191.
- [85] Weigend, F.; Ahlrichs, R. *Phys. Chem. Chem. Phys.* **2005**, *7*, 3297–3305.
- [86] Wheeler, S. E.; Houk, K. N.; Schleyer, P. v. R.; Allen, W. D. *J. Am. Chem. Soc.* **2009**, *131*, 2547–2560.
- [87] Wiberg, K. B. *Tetrahedron* **1968**, *24*, 1083–1096.
- [88] Tsumuraya, T.; Batcheller, S.; Masamune, S. *Angew. Chem. Int. Ed.* **1991**, *30*, 902–930.

- [89] Driess, M.; Grutzmacher, H. *Angew. Chem. Int. Ed.* **1996**, *35*, 829–856.
- [90] Power, P. P. *Chem. Rev.* **1999**, *99*, 3463–3504.
- [91] Sekiguchi, A.; Tsukamoto, M.; Ichinohe, M. *Science* **1997**, *275*, 60–61.
- [92] Schleyer, P. v. R. *Science* **1997**, *275*, 39–40.
- [93] Lee, V. Y.; Sekiguchi, A. *Angew. Chem. Int. Ed.* **2007**, *46*, 6596–6620.
- [94] Lee, V. Y.; Sekiguchi, A. *Acc. Chem. Res.* **2007**, *40*, 410–419.
- [95] Mizuhata, Y.; Sasamori, T.; Tokitoh, N. *Chem. Rev.* **2009**, *109*, 3479–3511.
- [96] Lavallo, V.; Canac, Y.; Donnadieu, B.; Schoeller, W. W.; Bertrand, G. *Science* **2006**, *312*, 722–4.
- [97] Mandal, S. K.; Roesky, H. W. *Chem. Commun.* **2010**, *46*, 6016–6041.
- [98] Reisenauer, H. P.; Maier, G.; Riemann, A.; Hoffmann, R. W. *Angew. Chem. Int. Ed.* **1984**, *23*, 641–641.
- [99] Seburg, R. a.; Patterson, E. V.; Stanton, J. F.; McMahon, R. J. *J. Am. Chem. Soc.* **1997**, *119*, 5847–5856.
- [100] Seburg, R. A.; McMahon, R. J. *Angew. Chem. Int. Ed.* **1995**, *34*, 2009–2012.
- [101] Achkasova, E.; Araki, M.; Denisov, A.; Maier, J. P. *J. Mol. Spec.* **2006**, *237*, 70–75.
- [102] Hemberger, P.; Noller, B.; Steinbauer, M.; Fischer, K.; Fischer, I. *J. Phys. Chem. Lett* **2010**, *1*, 228–231.
- [103] Lee, T. J.; Bunge, A.; Schaefer, H. F. *J. Am. Chem. Soc.* **1985**, *107*, 137–142.

- [104] Rubio, M.; Stålring, J.; Bernhardsson, A.; Lindh, R.; Roos, B. O. *Theor. Chem. Acc.* **2000**, *105*, 15–30.
- [105] Wu, Q.; Cheng, Q.; Yamaguchi, Y.; Li, Q.; Schaefer, H. F. *J. Chem. Phys.* **2010**, *132*, 044308.
- [106] Frenking, G.; Remington, R. B.; Schaefer, H. F. *J. Am. Chem. Soc.* **1986**, *108*, 2169–2173.
- [107] Maier, G.; Reisenauer, H. P.; Pacl, H. *Angew. Chem. Int. Ed.* **1994**, *33*, 1248–1250.
- [108] Maier, G.; Pacl, H.; Reisenauer, H. P.; Meudt, A.; Janoschek, R. *J. Am. Chem. Soc.* **1995**, *117*, 12712–12720.
- [109] Maier, G.; Reisenauer, H.; Egenolf, H. *Eur. J. Org. Chem.* **1998**, 1313–1317.
- [110] Vacek, G.; Colegrove, B. T.; Schaefer, H. F. *J. Am. Chem. Soc.* **1991**, *113*, 3192–3193.
- [111] Sherrill, C. D.; Brandow, C. G.; Allen, W. D.; Schaefer, H. F. *J. Am. Chem. Soc.* **1996**, *118*, 7158–7163.
- [112] Ikuta, S.; Saitoh, T.; Wakamatsu, S. *J. Chem. Phys.* **2004**, *121*, 3478–85.
- [113] Thorwirth, S.; Harding, M. E. *J. Chem. Phys.* **2009**, *130*, 214303.
- [114] Wu, Q.; Simmonett, A. C.; Yamaguchi, Y.; Li, Q.; Schaefer, H. F. *J. Phys. Chem. C* **2010**, *114*, 5447–5457.
- [115] Jemmis, E. D.; Prasad, B. V.; Tsuzuki, S.; Tanabe, K. *J. Phys. Chem.* **1990**, *94*, 5530–5535.
- [116] Ikuta, S.; Wakamatsu, S. *J. Chem. Phys.* **2004**, *120*, 11071–81.

- [117] Wu, Q.; Hao, Q.; Yamaguchi, Y.; Li, Q.; Fang, D.-C.; Schaefer, H. F. *J. Phys. Chem. A* **2010**, *114*, 7102–9.
- [118] Lu, T.; Wilke, J. J.; Yamaguchi, Y.; Schaefer, H. F. *J. Chem. Phys.* **2011**, *134*, 164101–164107.
- [119] Teng, Y.-L.; Xu, Q. *J. Phys. Chem. A* **2009**, *113*, 12163–70.
- [120] Hao, Q.; Simmonett, A. C.; Yamaguchi, Y.; Fang, D.-C.; Schaefer, H. F. *J. Comp. Chem.* **2011**, *32*, 15–22.
- [121] Saunders, M. *J. Comp. Chem.* **2004**, *25*, 621–624.
- [122] Bera, P. P.; Sattelmeyer, K. W.; Saunders, M.; Schaefer, H. F.; Schleyer, P. v. R. *J. Phys. Chem. A* **2006**, *110*, 4287–4290.
- [123] Wheeler, S. E.; v. R. Schleyer, P.; Schaefer, H. F. *J. Chem. Phys.* **2007**, *126*, 104104.
- [124] "Advances in methods and algorithms in a modern quantum chemistry program package", Shao, Y.; Fusti-Molnar, L.; Jung, Y.; Kussmann, J.; Ochsenfeld, C.; Brown, S. T.; Gilbert, A. T. B.; Slipchenko, L. V.; Levchenko, S. V.; O'Neill, D. P.; Distasio Jr., R. A.; Lochan, R. C.; Wang, T.; Beran, G. J. O.; Besley, N. A.; Herbert, J. M.; Lin, C. Y.; Van Voorhis, T.; Chien, S. H.; Sodt, A. R.; Steele, P.; Rassolov, V. A.; Maslen, P. E.; Korambath, P. P.; Adamson, R. D.; Austin, B.; Baker, J.; Byrd, E. F. C.; Dachsel, H.; Doerksen, R. J.; Dreuw, A.; Dunietz, B. D.; Dutoi, A. D.; Furlani, T. R.; Gwaltney, S. R.; Heyden, A.; Hirata, S.; Hsu, C.-P.; Kedziora, G.; Khalliulin, R. Z.; Klunzinger P.; Lee, A. M.; Lee, M. S.; Liang, W.; Lotan, I.; Nair, N.; Peters, B.; Proynov, E. I.; Pieniazek, P. A.; Rhee, Y. M.; Ritchie, J.; Rosta, E.; Sherrill, C. D.; Simmonett, A. C.; Subotnik, J. E.; Woodcock III, H. L.; Zhang, W.; Bell, A. T.; Chakraborty, A. K.; Chipman, D. M.; Keil, F. J.; Warshel, A.; Hehre, W. J.; Schaefer, H. F.; Kong, J.;

- Krylov, A. I.; Gill, P. M. W.; Head-Gordon, M. *Phys. Chem. Chem. Phys.*, 2006, 8, 3172 - 3191.
- [125] Raghavachari, K.; Trucks, G. W.; Pople, J. A.; Head-Gordon, M. *Chem. Phys. Lett.* **1989**, 157, 479–483.
- [126] Stanton, J. F. *Chem. Phys. Lett.* **1997**, 281, 130–134.
- [127] Watts, J. D.; Gauss, J.; Bartlett, R. J. *Chem. Phys. Lett.* **1992**, 200, 1–2.
- [128] Siegbahn, P.; Heiberg, A.; Roos, B.; Levy, B. *Phys. Scr.* **1980**, 21, 323–327.
- [129] Roos, B.; Taylor, P.; Siegbahn, P. E. M. *Chem. Phys.* **1980**, 48, 157–173.
- [130] Löwdin, P.-O.; Shull, H. *Phys. Rev.* **1956**, 101, 1730–1739.
- [131] Kállay, M.; Gauss, J. *J. Chem. Phys.* **2005**, 123, 214105–214117.
- [132] Kállay, M.; Surján, P. *J. Chem. Phys.* **2001**, 115, 2945–2954.
- [133] Helgaker, T.; Klopper, W.; Koch, H.; Noga, J. *J. Chem. Phys.* **1997**, 106, 9639–9646.
- [134] Feller, D. *J. Chem. Phys.* **1993**, 98, 7059–7071.
- [135] CFOUR, a quantum chemical program package written by Stanton, J.F.; Gauss, J.; Watts, J.D.; Szalay, P.G.; Bartlett, R.J. with contributions from Auer, A.A.; Bernholdt, D.E.; Christiansen, O.; Harding, M.E.; Heckert, M.; Heun, O.; Huber, C.; Jonsson, D.; Jusélius, J.; Lauderdale, W.J.; Metzroth, T.; Michauk, C.; O’Neill, D.P.; Price, D.R.; Ruud, K.; Schiffmann, F.; Tajti, A.; Varner, M.E.; Vázquez, J. and the integral packages: MOLECULE ( Almlöf, J. and Taylor, P.R.), PROPS ( Taylor, P.R.), ABACUS ( Helgaker, T.; Jensen, H.J. Aa.; Jørgensen, P.; and Olsen, J.), and ECP routines by Mitin, A.V. and van Wüllen, C. . For the current version see, <http://www.cfour.de>.

- [136] MOLPRO, version 2006.1, a package of ab initio programs, Werner, H.-J.; Knowles, P.J.; Lindh, R.; Manby, F.R.; Schütz, M.; Celani, P.; Korona, T.; Rauhut, G.; Amos, R.D.; Bernhardsson, A. ; Berning, A. ; Cooper, D.L. ; Deegan, M.J.O.; Dobbyn, A.J.; Eckert, F.; Hampel, C.; Hetzer, G.; Lloyd, A.W.; McNicholas, S.J.; Meyer, W.; Mura, M.E.; Nicklass, A.; Palmieri, P.; Pitzer, R.; Schumann, U.; Stoll, H.; Stone, A.J.; Tarroni, R.; Thorsteinsson, T. see <http://www.molpro.net>.
- [137] Schleyer, P. v. R.; Maerker, C.; Dransfeld, A.; Jiao, H.; Hommes, N. J. R. V. E. *J. Am. Chem. Soc.* **1996**, *118*, 6317–6318.
- [138] Chen, Z.; Wannere, C. S.; Corminboeuf, C.; Puchta, R.; Schleyer, P. V. R. *Chem. Rev.* **2005**, *105*, 3842–3888.
- [139] Fallah-Bagher-Shaidaei, H.; Wannere, C. S.; Corminboeuf, C.; Puchta, R.; Schleyer, P. v. R. *Org. Lett.* **2006**, *8*, 863–866.
- [140] Perez, N.; Heine, T.; Barthel, R.; Seifert, G.; Vela, A.; Mendez-Rojas, M.; Merino, G. *Org. Lett.* **2005**, *7*, 1509–1512.
- [141] Collins, J. B.; Dill, J. D.; Jemmis, E. D.; Apeloig, Y.; Schleyer, P. v. R.; Seeger, R.; Pople, J. A. *J. Am. Chem. Soc.* **1976**, *98*, 5419–5427.
- [142] Schleyer, P. v. R.; Boldyrev, A. I. *J. Chem. Soc., Chem. Commun.* **1991**, *0*, 1536–1538.
- [143] Minyaev, R. M.; Gribanova, T. N.; Minkin, V. I.; Starikov, A. G.; Hoffmann, R. *J. Org. Chem.* **2005**, *70*, 6693–704.

# Appendices



# Appendix A

## Supporting Information for Chapter 3

### A.1 Focal point table for stationary points 4S - SSP2

Table A.1: Focal point table for the 4S isomer

	HF	+ $\delta$ MP2	+ $\delta$ CCSD	+ $\delta$ CCSD(T)	+ $\delta$ CCSDT	+ $\delta$ CCSDT(Q)	NET
cc-pVDZ	+36.20	+2.13	-5.64	-1.44	-0.42	-0.67	[+30.16]
cc-pVTZ	+36.49	+3.37	-5.12	-1.50	[-0.42]	[-0.67]	[+32.16]
cc-pVQZ	+36.53	+3.53	-4.75	-1.55	[-0.42]	[-0.67]	[+32.68]
cc-pV5Z	+36.52	+2.66	[-4.75]	[-1.55]	[-0.42]	[-0.67]	[+31.80]
CBS LIMIT	[+36.52]	[+1.74]	[-4.75]	[-1.55]	[-0.42]	[-0.67]	[+ <b>30.88</b> ]
$\Delta E_{final} = \Delta E_e[\text{CCSDT(Q)/CBS}] + \Delta_{\text{ZPVE}}[\text{CCSD(T)/cc-pVQZ}] + \Delta_{\text{core}}[\text{CCSD(T)/cc-pCVQZ}] + \Delta_{\text{DBOC}}[\text{CCSD(T)/cc-pVQZ}] + \Delta_{\text{rel}}[\text{CCSD(T)/cc-pVQZ}]$ $= 30.88 + 1.13 - 0.68 - 0.01 + 0.37 = \mathbf{31.69 \text{ kcal mol}^{-1}}$							

<sup>a</sup>The symbol  $\delta$  denotes the increment in the relative energy ( $\Delta E_e$ ) with respect to the preceding level of theory in the hierarchy RHF $\rightarrow$ MP2 $\rightarrow$ CCSD $\rightarrow$ CCSD(T) $\rightarrow$ CCSDT $\rightarrow$ CCSDT(Q). Square brackets signify results obtained from basis set extrapolations or additivity assumptions. Final predictions are boldfaced.

Table A.2: Focal point table for the 5S isomer

	HF	+ $\delta$ MP2	+ $\delta$ CCSD	+ $\delta$ CCSD(T)	+ $\delta$ CCSDT	+ $\delta$ CCSDT(Q)	NET
cc-pVDZ	+39.71	-0.84	+1.30	-1.02	+0.02	-0.28	[+38.89]
cc-pVTZ	+40.25	-0.68	+1.27	-0.69	[+0.02]	[-0.28]	[+39.90]
cc-pVQZ	+39.89	-1.46	+1.10	-0.62	[+0.02]	[-0.28]	[+38.66]
cc-pV5Z	+39.88	-0.57	[+1.10]	[-0.62]	[+0.02]	[-0.28]	[+39.55]
CBS LIMIT	[+39.89]	[+0.37]	[+1.10]	[-0.62]	[+0.02]	[-0.28]	[+ <b>40.50</b> ]
$\Delta E_{final} = \Delta E_e[\text{CCSDT(Q)/CBS}] + \Delta_{\text{ZPVE}}[\text{CCSD(T)/cc-pVQZ}] + \Delta_{\text{core}}[\text{CCSD(T)/cc-pCVQZ}] + \Delta_{\text{DBOC}}[\text{CCSD(T)/cc-pVQZ}] + \Delta_{\text{rel}}[\text{CCSD(T)/cc-pVQZ}]$ $= 40.50 - 1.83 - 0.63 - 0.01 + 1.86 = \mathbf{39.89 \text{ kcal mol}^{-1}}$							

<sup>a</sup>The symbol  $\delta$  denotes the increment in the relative energy ( $\Delta E_e$ ) with respect to the preceding level of theory in the hierarchy RHF $\rightarrow$ MP2 $\rightarrow$ CCSD $\rightarrow$ CCSD(T) $\rightarrow$ CCSDT $\rightarrow$ CCSDT(Q). Square brackets signify results obtained from basis set extrapolations or additivity assumptions. Final predictions are boldfaced.

**Table A.3:** Focal point table for the **6S** isomer

	HF	+ $\delta$ MP2	+ $\delta$ CCSD	+ $\delta$ CCSD(T)	+ $\delta$ CCSDT	+ $\delta$ CCSDT(Q)	NET
cc-pVDZ	+57.92	+14.26	-11.38	-0.93	-0.89	-0.41	[+58.56]
cc-pVTZ	+59.97	+14.02	-11.34	-0.58	[-0.89]	[-0.41]	[+60.75]
cc-pVQZ	+59.92	+13.94	-11.34	-0.53	[-0.89]	[-0.41]	[+60.69]
cc-pV5Z	+59.96	+14.07	[-11.34]	[-0.53]	[-0.89]	[-0.41]	[+60.86]
CBS LIMIT	[+59.97]	[+14.21]	[-11.34]	[-0.53]	[-0.89]	[-0.41]	[+ <b>61.02</b> ]
$\Delta E_{final} = \Delta E_e[\text{CCSDT(Q)}/\text{CBS}] + \Delta_{\text{ZPVE}}[\text{CCSD(T)}/\text{cc-pVQZ}] + \Delta_{\text{core}}[\text{CCSD(T)}/\text{cc-pCVQZ}] + \Delta_{\text{DBOC}}[\text{CCSD(T)}/\text{cc-pVQZ}] + \Delta_{\text{rel}}[\text{CCSD(T)}/\text{cc-pVQZ}]$ $= 61.02 - 3.64 - 0.21 - 0.04 + 0.94 = \mathbf{58.05 \text{ kcal mol}^{-1}}$							

<sup>a</sup>The symbol  $\delta$  denotes the increment in the relative energy ( $\Delta E_e$ ) with respect to the preceding level of theory in the hierarchy RHF $\rightarrow$ MP2 $\rightarrow$ CCSD $\rightarrow$ CCSD(T) $\rightarrow$ CCSDT $\rightarrow$ CCSDT(Q). Square brackets signify results obtained from basis set extrapolations or additivity assumptions. Final predictions are boldfaced.

**Table A.4:** Focal point table for the **7S** isomer

	HF	+ $\delta$ MP2	+ $\delta$ CCSD	+ $\delta$ CCSD(T)	+ $\delta$ CCSDT	+ $\delta$ CCSDT(Q)	NET
cc-pVDZ	+102.01	-13.78	+3.03	-4.18	+0.23	-0.80	[+86.50]
cc-pVTZ	+102.75	-14.82	+4.23	-4.31	[+0.23]	[-0.80]	[+87.28]
cc-pVQZ	+102.62	-15.88	+4.59	-4.42	[+0.23]	[-0.80]	[+86.34]
cc-pV5Z	+102.59	-16.61	[+4.59]	[-4.42]	[+0.23]	[-0.80]	[+85.57]
CBS LIMIT	[+102.58]	[-17.38]	[+4.59]	[-4.42]	[+0.23]	[-0.80]	[+ <b>84.80</b> ]
$\Delta E_{final} = \Delta E_e[\text{CCSDT(Q)}/\text{CBS}] + \Delta_{\text{ZPVE}}[\text{CCSD(T)}/\text{cc-pVQZ}] + \Delta_{\text{core}}[\text{CCSD(T)}/\text{cc-pCVQZ}] + \Delta_{\text{DBOC}}[\text{CCSD(T)}/\text{cc-pVQZ}] + \Delta_{\text{rel}}[\text{CCSD(T)}/\text{cc-pVQZ}]$ $= 84.80 - 3.74 - 0.20 - 0.04 + 1.29 = \mathbf{82.11 \text{ kcal mol}^{-1}}$							

<sup>a</sup>The symbol  $\delta$  denotes the increment in the relative energy ( $\Delta E_e$ ) with respect to the preceding level of theory in the hierarchy RHF $\rightarrow$ MP2 $\rightarrow$ CCSD $\rightarrow$ CCSD(T) $\rightarrow$ CCSDT $\rightarrow$ CCSDT(Q). Square brackets signify results obtained from basis set extrapolations or additivity assumptions. Final predictions are boldfaced.

**Table A.5:** Focal point table for the **TS1** stationary point

	HF	+ $\delta$ MP2	+ $\delta$ CCSD	+ $\delta$ CCSD(T)	+ $\delta$ CCSDT	+ $\delta$ CCSDT(Q)	NET
cc-pVDZ	+22.65	-2.90	+0.52	-0.67	+0.07	-0.15	[+19.51]
cc-pVTZ	+22.15	-2.99	+0.93	-0.88	[+0.07]	[-0.15]	[+19.13]
cc-pVQZ	+22.38	-3.75	+1.27	-0.97	[+0.07]	[-0.15]	[+18.85]
cc-pV5Z	+22.36	-3.99	[+1.27]	[-0.97]	[+0.07]	[-0.15]	[+18.60]
CBS LIMIT	[+22.35]	[-4.24]	[+1.27]	[-0.97]	[+0.07]	[-0.15]	[+ <b>18.33</b> ]
$\Delta E_{final} = \Delta E_e[\text{CCSDT(Q)}/\text{CBS}] + \Delta_{\text{ZPVE}}[\text{CCSD(T)}/\text{cc-pVQZ}] + \Delta_{\text{core}}[\text{CCSD(T)}/\text{cc-pCVQZ}] + \Delta_{\text{DBOC}}[\text{CCSD(T)}/\text{cc-pVQZ}] + \Delta_{\text{rel}}[\text{CCSD(T)}/\text{cc-pVQZ}]$ $= 18.33 + 0.36 - 0.41 + 0.03 - 0.47 = \mathbf{18.11 \text{ kcal mol}^{-1}}$							

<sup>a</sup>The symbol  $\delta$  denotes the increment in the relative energy ( $\Delta E_e$ ) with respect to the preceding level of theory in the hierarchy RHF $\rightarrow$ MP2 $\rightarrow$ CCSD $\rightarrow$ CCSD(T) $\rightarrow$ CCSDT $\rightarrow$ CCSDT(Q). Square brackets signify results obtained from basis set extrapolations or additivity assumptions. Final predictions are boldfaced.

**Table A.6:** Focal point table for the **TS2** stationary point

	HF	+ $\delta$ MP2	+ $\delta$ CCSD	+ $\delta$ CCSD(T)	+ $\delta$ CCSDT	+ $\delta$ CCSDT(Q)	NET
cc-pVDZ	+98.08	-2.78	+0.54	-2.56	-0.03	-0.30	[+92.94]
cc-pVTZ	+97.80	-5.05	+0.83	-2.68	[-0.03]	[-0.30]	[+90.57]
cc-pVQZ	+97.54	-5.42	+0.65	-2.81	[-0.03]	[-0.30]	[+89.63]
cc-pV5Z	+97.51	-6.27	[+0.65]	[-2.81]	[-0.03]	[-0.30]	[+88.75]
CBS LIMIT	[+97.51]	[-7.16]	[+0.65]	[-2.81]	[-0.03]	[-0.30]	[+ <b>87.85</b> ]
$\Delta E_{final} = \Delta E_e[\text{CCSDT(Q)}/\text{CBS}] + \Delta_{\text{ZPVE}}[\text{CCSD(T)}/\text{cc-pVQZ}] + \Delta_{\text{core}}[\text{CCSD(T)}/\text{cc-pCVQZ}] + \Delta_{\text{DBOC}}[\text{CCSD(T)}/\text{cc-pVQZ}] + \Delta_{\text{rel}}[\text{CCSD(T)}/\text{cc-pVQZ}]$ $= 87.85 - 3.43 + 0.69 + 3.16 = \mathbf{88.27 \text{ kcal mol}^{-1}}$							

<sup>a</sup>The symbol  $\delta$  denotes the increment in the relative energy ( $\Delta E_e$ ) with respect to the preceding level of theory in the hierarchy RHF $\rightarrow$ MP2 $\rightarrow$ CCSD $\rightarrow$ CCSD(T) $\rightarrow$ CCSDT $\rightarrow$ CCSDT(Q). Square brackets signify results obtained from basis set extrapolations or additivity assumptions. Final predictions are boldfaced.

**Table A.7:** Focal point table for the **SSP1** stationary point

	HF	+ $\delta$ MP2	+ $\delta$ CCSD	+ $\delta$ CCSD(T)	+ $\delta$ CCSDT	+ $\delta$ CCSDT(Q)	NET
cc-pVDZ	+16.67	+12.26	-6.76	+2.48	-0.26	+0.25	[+24.64]
cc-pVTZ	+16.59	+13.00	-6.61	+2.42	[-0.26]	[+0.25]	[+25.39]
cc-pVQZ	+16.96	+12.38	-6.37	+2.41	[-0.26]	[+0.25]	[+25.36]
cc-pV5Z	+16.93	+11.90	[-6.37]	[+2.41]	[-0.26]	[+0.25]	[+24.86]
CBS LIMIT	[+16.91]	[+11.41]	[-6.37]	[+2.41]	[-0.26]	[+0.25]	[+ <b>24.34</b> ]
$\Delta E_{final} = \Delta E_e[\text{CCSDT(Q)}/\text{CBS}] + \Delta_{\text{ZPVE}}[\text{CCSD(T)}/\text{cc-pVQZ}] + \Delta_{\text{core}}[\text{CCSD(T)}/\text{cc-pCVQZ}] + \Delta_{\text{DBOC}}[\text{CCSD(T)}/\text{cc-pVQZ}] + \Delta_{\text{rel}}[\text{CCSD(T)}/\text{cc-pVQZ}]$ $= 24.34 - 0.03 - 1.73 - 0.04 + 0.03 = \mathbf{22.57 \text{ kcal mol}^{-1}}$							

<sup>a</sup>The symbol  $\delta$  denotes the increment in the relative energy ( $\Delta E_e$ ) with respect to the preceding level of theory in the hierarchy RHF $\rightarrow$ MP2 $\rightarrow$ CCSD $\rightarrow$ CCSD(T) $\rightarrow$ CCSDT $\rightarrow$ CCSDT(Q). Square brackets signify results obtained from basis set extrapolations or additivity assumptions. Final predictions are boldfaced.

**Table A.8:** Focal point table for the **SSP2** stationary point

	HF	+ $\delta$ MP2	+ $\delta$ CCSD	+ $\delta$ CCSD(T)	+ $\delta$ CCSDT	+ $\delta$ CCSDT(Q)	NET
cc-pVDZ	+124.63	+0.27	-12.05	-6.03	-0.41	-2.62	[+103.80]
cc-pVTZ	+126.59	+0.89	-11.76	-6.21	[-0.41]	[-2.62]	[+106.49]
cc-pVQZ	+126.54	+1.40	-11.73	-6.31	[-0.41]	[-2.62]	[+106.88]
cc-pV5Z	+126.65	+0.75	[-11.73]	[-6.31]	[-0.41]	[-2.62]	[+106.34]
CBS LIMIT	[+126.69]	[+0.07]	[-11.73]	[-6.31]	[-0.41]	[-2.62]	[+ <b>105.69</b> ]
$\Delta E_{final} = \Delta E_e[\text{CCSDT(Q)}/\text{CBS}] + \Delta_{\text{ZPVE}}[\text{CCSD(T)}/\text{cc-pVQZ}] + \Delta_{\text{core}}[\text{CCSD(T)}/\text{cc-pCVQZ}] + \Delta_{\text{DBOC}}[\text{CCSD(T)}/\text{cc-pVQZ}] + \Delta_{\text{rel}}[\text{CCSD(T)}/\text{cc-pVQZ}]$ $= 105.69 - 3.41 - 0.68 - 0.02 + 2.15 = \mathbf{103.73 \text{ kcal mol}^{-1}}$							

<sup>a</sup>The symbol  $\delta$  denotes the increment in the relative energy ( $\Delta E_e$ ) with respect to the preceding level of theory in the hierarchy RHF $\rightarrow$ MP2 $\rightarrow$ CCSD $\rightarrow$ CCSD(T) $\rightarrow$ CCSDT $\rightarrow$ CCSDT(Q). Square brackets signify results obtained from basis set extrapolations or additivity assumptions. Final predictions are boldfaced.

## A.2 Natural Bond Orbital Analysis

Table A.9: Natural bond orbitals for isomer **1S** obtained at the B3LYP/def2-TZVP level of theory

Bond	Type	Occupancy	NBO	%p and %s
Ge3	LP	1.94963	$\text{sp}^{0.19}(\text{Ge3})$	Ge3: 16.28% p 83.67% s
Ge4	LP	1.94963	$\text{sp}^{0.19}(\text{Ge4})$	Ge4: 16.28% p 83.67% s
C1-H2	BD	1.99359	$0.7878\text{sp}^{1.74}(\text{C1})+0.6159\text{sp}^{0.00}(\text{H2})$	C1: 63.39% p 36.49% s H2: 0.09% p 99.91% s
C1-Ge4	BD	1.97302	$0.8609\text{sp}^{2.15}(\text{C1})+0.5087\text{sp}^{6.44}(\text{Ge4})$	C1: 68.04% p 31.61% s Ge4: 86.28% p 13.40% s
C1-Ge3	BD	1.97302	$0.8609\text{sp}^{2.15}(\text{C1})+0.5087\text{sp}^{6.44}(\text{Ge3})$	C1: 68.04% p 31.61% s Ge3: 86.28% p 13.40% s
C1-Ge3-Ge4	3C	1.99940	$0.7803\text{sp}^{1.00}(\text{C1})+0.4422\text{sp}^{1.00}(\text{Ge3})+0.4422\text{sp}^{1.00}(\text{Ge4})$	C1: 99.48% p 0.00% s Ge3: 98.94% p 0.00% s Ge4: 98.94% p 0.00% s
Ge3-Ge4-H5	3C	1.97344	$0.4334\text{sp}^{24.47}(\text{Ge3})+0.4334\text{sp}^{24.47}(\text{Ge4})+0.7902\text{sp}^{0.00}(\text{H5})$	Ge3: 95.29% p 3.89% s Ge4: 95.29% p 3.89% s H5: 0.25% p 99.75% s

Table A.10: Natural bond orbitals for isomer **2S** obtained at the B3LYP/def2-TZVP level of theory

Bond	Type	Occupancy	NBO	%p and %s
Ge3	LP	1.96675	$\text{sp}^{0.16}(\text{Ge3})$	Ge3: 13.54% p 86.43% s
C1-Ge2	BD	1.99369	$0.8411\text{sp}^{2.00}(\text{C1})+0.5408\text{sp}^{7.08}(\text{Ge2})$	C1: 66.46% p 33.23% s Ge2: 87.44% p 12.35% s
Ge2-Ge3	BD	1.87388	$0.8809\text{sp}^{1.16}(\text{Ge2})+0.4733\text{sp}^{46.55}(\text{Ge3})$	Ge2: 53.56% p 46.37% s Ge3: 97.29% p 2.09% s
C1-Ge2-Ge3	3C	1.99984	$0.7514\text{sp}^{1.00}(\text{C1})+0.4789\text{sp}^{1.00}(\text{Ge2})+0.4540\text{sp}^{1.00}(\text{Ge3})$	C1: 99.34% p 0.00% s Ge2: 99.32% p 0.00% s Ge3: 99.04% p 0.00% s
C1-Ge3	BD	1.98553	$0.8632\text{sp}^{2.38}(\text{C1})+0.5048\text{sp}^{7.29}(\text{Ge3})$	C1: 70.14% p 29.46% s Ge3: 87.65% p 12.02% s
C1-H5	BD	1.99479	$0.7867\text{sp}^{1.70}(\text{C1})+0.6173\text{sp}^{0.00}(\text{H5})$	C1: 62.91% p 36.97% s H5: 0.08% p 99.92% s
Ge2-H4	BD	1.96960	$0.6760\text{sp}^{1.39}(\text{Ge2})+0.7369\text{sp}^{0.00}(\text{H4})$	Ge2: 58.13% p 41.70% s H4: 0.17% p 99.83% s

Table A.11: Natural bond orbitals for isomer **3S** obtained at the B3LYP/def2-TZVP level of theory

Bond	Type	Occupancy	NBO	%p and %s
Ge2	LP	1.96138	$\text{sp}^{0.15}(\text{Ge2})$	Ge2: 13.11% p 86.85% s
Ge1	LP	1.98211	$\text{sp}^{0.14}(\text{Ge1})$	Ge1: 12.01% p 87.97% s
Ge1-Ge2-C3	3C	1.99278	$0.2724\text{sp}^{14.33}(\text{Ge1})+0.4334\text{sp}^{9.73}(\text{Ge2})+0.8590\text{sp}^{1.03}(\text{C3})$	Ge1: 92.49% p 6.45% s Ge2: 90.08% p 92.49% s C3: 50.54% p 49.14% s
Ge1-Ge2-C3	3C	1.99958	$0.4394\text{sp}^{1.00}(\text{Ge1})+0.4182\text{sp}^{1.00}(\text{Ge2})+0.7951\text{sp}^{1.00}(\text{C3})$	Ge1: 98.80% p 0.00% s Ge2: 98.91% p 0.00% s C3: 99.59% p 0.00% s
C3-H4	BD	1.97424	$0.7989\text{sp}^{2.20}(\text{C3})+0.6014\text{sp}^{0.00}(\text{H4})$	C3: 68.66% p 31.17% s H4: 0.03% p 99.97% s
Ge1-Ge2	BD	1.93439	$0.7287\text{sp}^{11.98}(\text{Ge1})+0.6848\text{sp}^{18.77}(\text{Ge2})$	Ge1: 91.84% p 7.67% s Ge2: 94.27% p 5.02% s
C3-H5	BD	1.91659	$0.7889\text{sp}^{4.17}(\text{C3})+0.6145\text{sp}^{0.00}(\text{H5})$	C3: 80.27% p 19.25% s H5: 0.11% p 99.89% s